

1 TORC2 dependent phosphorylation modulates calcium  
2 regulation of fission yeast myosin.

3

4

5

6

7 Karen Baker<sup>1</sup>, Irene A. Gyamfi<sup>1</sup>, Gregory I. Mashanov<sup>2</sup>, Justin E. Molloy<sup>2</sup>,  
8 Michael A. Geeves<sup>1</sup> and Daniel P. Mulvihill<sup>1,3</sup>

9

10

11 <sup>1</sup> School of Biosciences, University of Kent, Canterbury, Kent, CT2 7NJ, UK.

12

13 <sup>2</sup> The Francis Crick Institute, 1 Midland Road, London NW1 1AT, UK

14

15 <sup>3</sup> Author for correspondence e-mail: [d.p.mulvihill@kent.ac.uk](mailto:d.p.mulvihill@kent.ac.uk)

16

Tel: +44 (0) 1227 827239

17

18

19

20

21 Key words: pombe, endocytosis, calmodulin, Tor kinase.

22

23

24

25 Running Title: Phosphorylation & calcium co-dependent myosin regulation

26

27

28

29

30 **Abstract**

31 All cells have the ability to respond to changes in their environment. Signalling  
32 networks modulate cytoskeleton and membrane organisation to impact cell  
33 cycle progression, polarised cell growth and multicellular development  
34 according to the environmental setting. Using diverse *in vitro*, *in vivo* and single  
35 molecule techniques we have explored the role of myosin-1 signalling in  
36 regulating endocytosis during both mitotic and meiotic cell cycles. We have  
37 established that a conserved serine within the neck region of the sole fission  
38 yeast myosin-1 is phosphorylated in a TORC2 dependent manner to modulate  
39 myosin function. Myo1 neck phosphorylation brings about a change in the  
40 conformation of the neck region and modifies its interaction with calmodulins,  
41 Myo1 dynamics at endocytic foci, and promotes calcium dependent switching  
42 between different calmodulin light chains. These data provide insight into a  
43 novel mechanism by which myosin neck phosphorylation modulates acto-  
44 myosin dynamics to control polarised cell growth in response to mitotic and  
45 meiotic cell-cycle progression and the cellular environment.

46

## 47 **Introduction**

48 The actin cytoskeleton underpins cellular organisation by maintaining cell  
49 shape and through the transmission of mechanical signals between the cell  
50 periphery and nucleus, to influence protein expression, organisation and  
51 cellular architecture in response to needs of the cell. Myosins, actin-associated  
52 motor-proteins, work in collaboration to facilitate global cytoskeletal  
53 organisation and a plethora of transport processes including cell migration,  
54 intracellular transport, tension sensing and cell division (O'Connell *et al*, 2007).  
55 While there are many classes of myosin, each contains an actin binding  
56 ATPase motor domain, which exerts force against actin, a lever arm or neck  
57 region that contains light chain binding IQ motifs, and a tail region which  
58 specifies cargo binding and other molecular interactions.

59 Although different classes of myosin perform very different cellular functions  
60 they all operate by the same basic mechanism, whereby the motor domain  
61 undergoes cyclical interactions with actin coupled to the breakdown of ATP.  
62 Each molecule of ATP that is converted to ADP and inorganic phosphate can  
63 generate movement along actin of between 5-25 nm and force of up to 5 pN.  
64 Regulation of acto-myosin motility is multi-faceted (Heissler & Sellers, 2016a),  
65 combining regulatory pathways operating via the actin track (historically called  
66 thin-filament regulation), or myosin-linked regulation (historically called thick  
67 filament regulation) which is often mediated via phosphorylation of the heavy  
68 chain or light chain(s) or by calcium-regulation of light chain binding (Heissler  
69 & Sellers, 2016b). It has been shown that phosphorylation at the conserved  
70 "TEDS" motif within the myosin motor domain of class 1 myosin affects acto-  
71 myosin interaction (Bement & Mooseker, 1995); phosphorylation within the tail  
72 region of class 5 myosin controls cargo binding (Rogers *et al*, 1999), whereas  
73 phosphorylation of class 2 myosin light chains and/or heavy chain can change  
74 the folded state of the heavy chain, affecting both actin interaction and ability to  
75 form filaments (Redowicz, 2001; Kendrick-Jones *et al*, 1987; Pasapera *et al*,  
76 2015). So, phosphoregulation of myosin can occur in the head, neck and tail  
77 regions and also the light chains and its effects are manifold and vary across  
78 myosin classes and between paralogues within the same class. Its effect on

79 motile function is still not fully understood for many myosins, especially within  
80 yeast (East & Mulvihill, 2011).

81 The fission yeast, *Schizosaccharomyces pombe*, genome encodes for 5  
82 myosin heavy chains from classes 1, 2, and 5 (Win *et al*, 2002), representing  
83 the basic subset of these actin-associated motor proteins found in eukaryotic  
84 cells. The single class 1 myosin, Myo1, is a 135 kDa protein, with motor domain,  
85 neck region (with two canonical IQ motifs) and a 49 kDa tail region containing  
86 a, so-called, tail-homology-2 domain, PH domain, SH3 domain and a carboxyl-  
87 terminal acidic region that associates with and activates the Arp2/3 complex to  
88 nucleate actin polymerisation (Lee *et al*, 2000). The myosin motor has a  
89 conserved TEDS site, phosphorylated by a Ste20 protein kinase, to modulate  
90 the protein's ability to associate with actin (Attanapola *et al*, 2009). Myo1  
91 associates with membranes, primarily at sites of cell growth, where it is required  
92 for endocytosis, actin organisation and spore formation (Sirotkin *et al*, 2005;  
93 Lee *et al*, 2000; Itadani *et al*, 2007).

94 Calmodulin or calmodulin-like light chains associate with the IQ motifs within  
95 the myosin neck, providing a mechanism to regulate the length and stiffness of  
96 the lever arm (Trybus *et al*, 2007) and behaviour of the motor domain (Adamek  
97 *et al*, 2008). Calmodulins are ubiquitous calcium binding proteins that associate  
98 with and regulate the cellular function of diverse proteins. Calcium associates  
99 with up to four EF hand motifs within the calmodulin molecule to bring about a  
100 change in its conformation to modulate its affinity for IQ motifs within binding  
101 partner proteins (Crivici & Ikura, 1995). *S. pombe* encodes for two calmodulin  
102 like proteins, Cam1 and Cam2 (Takeda & Yamamoto, 1987; Itadani *et al*, 2007).  
103 Cam1 is a typical calmodulin that associates with IQ domain containing proteins  
104 in a calcium dependent manner, to affect functions as diverse as endocytosis,  
105 spore formation, cell division or maintaining spindle pole body integrity (Takeda  
106 & Yamamoto, 1987; Moser *et al*, 1995; 1997; Itadani *et al*, 2010). Unlike Cam1,  
107 Cam2 is not essential and is predicted to be insensitive to calcium, however  
108 like Cam1 it has been reported to regulate Myo1 (Sammons *et al*, 2011; Itadani  
109 *et al*, 2007). While cells lacking Cam2 show defects in spore formation they  
110 have no significant growth-associated phenotypes during the vegetative growth  
111 cycle.

112 TOR (Target of Rapamycin) signaling plays a key role in modulating cell growth  
113 in response to changes in cell cycle status and environmental conditions  
114 (Laplante & Sabatini, 2012). The mTOR kinase forms two distinct protein  
115 complexes TOR complex 1 (TORC1) and TORC2, each defined by unique  
116 components that are highly conserved across species. While both TORC1 and  
117 TORC2 have been implicated in the control of cell migration and F-actin  
118 organisation (Liu & Parent, 2011), TORC2 plays a key role in regulating the  
119 actin cytoskeleton in yeasts, *Dictyostelium discoideum* and mammalian cells  
120 (Jacinto *et al*, 2004; Baker *et al*, 2016; Lee *et al*, 2005). While the basic principle  
121 of control of each regulatory signal (e.g. phosphorylation and calcium signalling)  
122 are understood, the interplay between parallel modes of regulation is relatively  
123 unknown. *S. pombe*, contains both TORC1 and TORC2 complexes (Petersen,  
124 2009).

125 In the current study, we have used molecular cell biological, biochemical and  
126 single molecule techniques to help identify and characterise a novel TORC2  
127 phosphorylation-dependent system for regulating calcium-dependent switching  
128 of different calmodulin light chain(s) binding to the neck region of Myo1. We  
129 have established the contribution that each calmodulin plays in regulating this  
130 conserved motor protein and how they affect the conformation of the myosin  
131 lever arm. We propose a concerted mechanism of regulation by both calcium  
132 and phosphorylation that controls motility and function of Myo1 in response to  
133 signals controlling cell cycle progression.

## 134 **Results**

### 135 **Fission yeast myosin-1 is phosphorylated within the IQ neck domain.**

136 Analysis of extracts from exponentially growing fission yeast cells indicates its  
137 sole class I myosin, Myo1, is subject to multiple phosphorylation events (**Figure**  
138 **1A**). Phosphoproteomics studies (Carpy *et al*, 2014; Wilson-Grady *et al*, 2008)  
139 revealed a conserved phosphoserine residue located within the IQ motif  
140 containing neck region of class I & V myosins (**Figure 1B**). The location of this  
141 AGC family kinase consensus phosphoserine site (Pearce *et al*, 2010) has the  
142 potential to impact myosin activity and function by affecting conformation of the  
143 lever arm as well as light chain binding. A phosphospecific antibody was raised  
144 to confirm phosphorylation of the Myo1 serine 742 (Myo1<sup>S742</sup>), and established  
145 that it is phosphorylated in a TORC2 signalling and growth media dependent  
146 manner (**Figure 1C-E**). Consistent with the TORC2 dependent pathway  
147 modulating cell growth in response to media quality (Petersen & Nurse, 2007),  
148 replacing the serine with a non-phosphorylatable alanine residue within  
149 *myo1.S742A* cells resulted in an inability to inhibit growth when cultured in  
150 media containing minimal nitrogen (**Figure 1F**).

151

### 152 **Phosphorylation modulates Myo1 lever arm length.**

153 As serine 742 lies within the IQ motif containing neck region of myosin-1, we  
154 explored whether Myo1<sup>S742</sup> phosphorylation affects calmodulin binding and  
155 conformation of the neck region. Isoforms of the Ca<sup>2+</sup> sensitive fission yeast  
156 calmodulin (Cam1 and Cam1.T6C) were isolated in their native amino-  
157 terminally (Nt) acetylated forms using bacteria co-expressing the fission yeast  
158 NatA amino- $\alpha$ -acetyl-transferase complex (Eastwood *et al*, 2017). A FRET  
159 based fusion was generated with CyPet donor and YPet acceptor fluorophores  
160 (Nguyen & Daugherty, 2005) juxtaposed around the Cam1 protein to monitor  
161 Ca<sup>2+</sup> dependent changes in Cam1 conformation (**Figure 2A**). This FRET-Cam1  
162 fusion (**Figure 2B**), and Nt-acetylated IAANS labelled Cam1.T6C (**Figure 2C**)  
163 established Ca<sup>2+</sup> binding brings about a change in the Cam1 conformation.  
164 Calculated pCa values for the Cam1-FRET (**Figure 2B** pCa<sub>50</sub>: 6.12), reflect  
165 global change in Cam1 conformation, while the IAANS dependent pCa (**Figure**

166 **2C** pCa<sub>50</sub>: 6.54) reflects Ca<sup>2+</sup> dependent changes in the local environment at  
167 the amino lobe of Cam1. Quin-2, fluorescence of which increases upon Ca<sup>2+</sup>  
168 binding (Tsien, 1980), was used to establish Ca<sup>2+</sup> ions release from Cam1 with  
169 3 distinct rate constants (137, 12.9 and 2.0 s<sup>-1</sup>) (**Figure 2D**).

170 To characterise Cam1 binding to the IQ neck region of the fission yeast myosin-  
171 1, recombinant FRET constructs were produced in which CyPet and YPet were  
172 separated by individual or both Myo1 IQ motifs (Myo1<sup>IQ1</sup>-FRET, Myo1<sup>IQ2</sup>-FRET,  
173 Myo1<sup>IQ12</sup>-FRET) (**Figure 2E & S1**). Cam1 binding to the IQ motif(s) stabilises  
174 the  $\alpha$ -helix and results in a calcium regulated drop in FRET signal (**Figure 2E-**  
175 **F**). Analysis of interactions between Cam1 and Myo1<sup>IQ12</sup>-FRET revealed Cam1  
176 molecules associated with the combined Myo1<sup>IQ12</sup> motifs with 2 distinct phases,  
177 each contributing 50% of the overall change in signal (**Figure 2G**). The first  
178 Cam1-Myo1<sup>IQ12</sup> binding event corresponds to an affinity of less than 0.1  $\mu$ M  
179 (binding was too tight to calculate affinity with higher precision), while the  
180 second event correlates with an approximately 10-fold weaker binding affinity  
181 (0.68  $\mu$ M). This association was seen to be sensitive to calcium (pCa of 5.87)  
182 (**Figure 2I**), illustrating Cam1 only associates with Myo1 in low cellular Ca<sup>2+</sup>  
183 concentrations. Interestingly while Cam1 was seen to bind tightly to Myo1<sup>IQ1</sup>  
184 alone ( $K_d < 0.1 \mu$ M), no detectable association was observed for the equivalent  
185 single Myo1<sup>IQ2</sup> motif (**Figure 2J**). Together these data are consistent with a  
186 sequential cooperative binding mechanism by which the stable residency of  
187 Cam1 in the first IQ position is required before calmodulin can bind to Myo1<sup>IQ2</sup>.

188 Replacing serine 742 within the IQ neck region with a phosphomimetic  
189 aspartate residue had no significant impact upon the affinity, calcium sensitivity  
190 or cooperative nature of the interaction between Myo1 and Cam1 (**Figure 2G**).  
191 However, the phosphomimetic replacement resulted in a change in maximum  
192 FRET signal upon Cam1 binding ( $F_{max}$  46.05 vs 31.64) (**Figure 2G & H**)  
193 indicating Myo1<sup>S742</sup> phosphorylation changes the conformation of the lever arm  
194 upon Cam1 binding, rather than modulating the affinity for Cam1.

195

## 196 **Phosphorylation regulates Myo1 dynamics and endocytosis.**

197 To explore *in vivo* Myo1 and calmodulin dynamics we generated prototroph S.

198 *pombe* strains in which endogenous *myo1*, *cam1*, or *cam2* genes were fused  
199 to cDNA encoding for monomeric fluorescent proteins (Figure 3A). Using high-  
200 speed (20 Hz) single molecule TIRF analysis we explored how Myo1<sup>S742</sup>  
201 phosphorylation impacts Myo1 and Cam1 dynamics and function within the cell.  
202 Myo1 and Cam1 associated with the cell membrane in two distinct ways: we  
203 observed rapid transient associations of single molecules at the cell membrane,  
204 characterised by low-intensity single stepwise changes in intensity as well  
205 longer endocytic events which were much brighter and had a very different  
206 time-course. Single molecules of Myo1 and Cam1 bound transiently at the cell  
207 membrane and moved with low mobility ( $0.03 \mu\text{m}^2\cdot\text{s}^{-1}$ ), ~10-times slower than  
208 diffusion of integral membrane proteins (Mashanov *et al*, 2010). The individual,  
209 diffraction-limited fluorescent spots appeared and disappeared in a stepwise  
210 fashion (i.e. within a single video frame). Event durations were exponentially  
211 distributed with mean lifetime of  $2.2 \text{ s}^{-1}$  ( $n = 152$ ) (Movie 1). In contrast, during  
212 endocytic events, the fluorescence signal increased gradually, rising to a peak  
213 amplitude consistent with ~45 molecules of mNeogreen.Myo1 (rate ~13  
214 molecules. $\text{s}^{-1}$ ), which dwelled for ~6 s, before falling to baseline (rate ~14  
215 molecules. $\text{s}^{-1}$ ) (Figure 3B, Movie 2). The estimated number of Myo1 molecules  
216 is lower than reported in an earlier study (Sirotkin *et al*, 2010) perhaps due to  
217 differences in imaging techniques, as TIRF imaging illuminates the specimen  
218 to a depth of ~100nm whereas confocal imaging would extend to > 400nm).  
219 The duration ( $T_{\text{dur}}$ ) of endocytic events (measured as described in the Methods)  
220 was  $13.84 \text{ s} \pm 0.39$  (mean  $\pm$  SEM,  $n=50$ ) (Figure 3C) and while there was  
221 significant variation in the maximum mNeogreen.Myo1 intensity ( $2373 \pm$   
222  $155$ ), there was no correlation between maximum intensity and event duration  
223 (Figure 3D). Fluorescence intensity dynamics of Cam1.GFP during endocytic  
224 events were similar to mNeogreen.Myo1, but  $T_{\text{dur}}$  was significantly shorter ( $P$   
225  $<0.0001$ ),  $10.99 \text{ s} \pm 0.21$  ( $n=52$ ) while the peak intensity was roughly double  
226 that measured for mNeogreen.Myo1 and equivalent to ~ 90 GFP molecules  
227 (Figure 3E) consistent with Cam1 occupying both IQ sites within the Myo1 neck  
228 region. The briefer event duration observed for Cam1 might be explained by  
229 Cam1 dissociating from Myo1 before Myo1 leaves the endocytic patch. This  
230 idea was confirmed using two-colour imaging of *mNeogreen.myo1*  
231 *cam1.mCherry* cells which showed Myo1 and Cam1 arrived simultaneously at



232 the endocytic patch, but Cam1.mCherry disassociated ~3 s before  
233 mNeogreen.Myo1 (Figure 3F, S2).

234 Analysis of Myo1 and Cam1 dynamics in *myo1.S742A* cells during endocytosis  
235 revealed Myo1<sup>S742A</sup> had average assembly/disassembly rates and plateau  
236 intensity identical to wild type Myo1, but T<sub>dur</sub> was 1.5 sec shorter (12.3s +/- 0.31  
237 n=67) (Figure 3G & S2). Consistent with the *in vitro* data, the *myo1.S742A*  
238 mutation did not impact on the ability of Cam1 molecules associating at both IQ  
239 motifs, as average assembly/disassembly rates, and plateau intensity for Cam1  
240 were the same in both wild type and *myo1.S742A* cells. However, we found  
241 that Myo1<sup>S742A</sup> and Cam1 proteins disassociated simultaneously and somewhat  
242 earlier during the endocytic event in this strain.

243 These TIRF imaging data were consistent with widefield 3D-timelapse imaging  
244 that showed lifetimes of Myo1 and Cam1 foci were shorter in *myo1.S742A* cells  
245 when compared to *myo1*<sup>+</sup> (Figure 3H). In contrast, while the *myo1.S742A* allele  
246 did not affect accumulation of Cam2 or LifeACT to sites of endocytosis (Figure  
247 3I), the rate of endocytosis differs between old end and new ends of *myo1*-  
248 *S742A* cells compared to wild type (Figure 4A). Therefore, while Myo1<sup>S742</sup>  
249 phosphorylation does not impact assembly of Myo1-Cam1 endocytic foci, it  
250 regulates myosin activity to change the function of the ensemble of endocytic  
251 proteins during bipolar growth.

252

253 **Myo1 S742 is phosphorylated in a cell cycle dependent manner to**  
254 **regulate polarised cell growth.**

255 Upon cell division fission yeast cells grow exclusively from the old cell end that  
256 existed in the parental cell. At a point during interphase (called New End Take  
257 Off -NETO) there is a transition to a bipolar growth (Mitchison & Nurse, 1985).  
258 This cell cycle switch in growth pattern correlates precisely with a parallel  
259 redistribution of endocytic actin patches (Marks & Hyams, 1985). As the  
260 *myo1.S742A* allele only affected actin dynamics at the old cell end during  
261 bipolar growth we examined whether this post-translational modification was  
262 subject to cell cycle dependent variance. Analysis of extracts from cell division  
263 cycle mutants arrested in G1 (*cdc10.v50* cells) or late G2 (*cdc25.22* cells)

264 revealed Myo1<sup>S742</sup> is phosphorylated in a cell cycle dependent manner (Figure  
265 4B). This was confirmed by monitoring Myo1<sup>S742</sup> phosphorylation in cells  
266 synchronised with respect to cell cycle progression (Figure S3). These data  
267 established that Myo1<sup>S742</sup> phosphorylation peaks in early interphase (G1 cells),  
268 prior to the transition to a bipolar growth pattern, and steadily decreases until  
269 becoming undetectable towards the end of G2. Analysis of growth kinetics  
270 revealed *myo1.S742A* cells grow slower than wild type (Figure 4C), and have  
271 a longer average length (*myo1*<sup>+</sup>: 9.77 ± 1.77 µm; *myo1.S742A*: 13.2 ± 2.47 µm.  
272 t-test >99% significance n>500). In addition, a significant proportion of  
273 *myo1.S742A* cells demonstrate polarity defects, with 24.7% of cells having a  
274 bent morphology (i.e. growth deviates by >5° from longitudinal axis), compared  
275 to 1% seen in wild type (Figure 4D-E). Consistent with these observations,  
276 *myo1.S742* mutants exhibit defects in the transition from monopolar to polar  
277 growth. Cell wall staining revealed a significantly higher proportion of  
278 *myo1.S742A* cells exhibit monopolar growth compared to equivalent wild type,  
279 indicating disruption in the switch from monopolar to bipolar growth (Figure 4E).  
280 This was confirmed by tracking the cellular distribution of the actin patch  
281 marker, Sla2/End4, following cell division. Sla2 failed to redistribute to the newly  
282 divided end of *myo1.S742A* cells during interphase (Figure 4F). Together these  
283 data show that cell cycle variation in Myo1<sup>S742</sup> phosphorylation modulates the  
284 myosin lever arm to regulate endocytosis and polarised growth.

285

### 286 **Cam2 associates with internalised endosomes and not Myo1 during** 287 **vegetative growth.**

288 Myo1 has been reported to associate with a second calmodulin like protein,  
289 Cam2, via its second IQ motif (Sammons *et al*, 2011). However, our data  
290 indicate Cam1 occupies both Myo1 IQ motifs during endocytosis. Widefield  
291 microscopy revealed Myo1 and Cam1 dynamics (Figure 5A) at endocytic foci  
292 differ significantly from Cam2 which is recruited to sites of endocytosis later  
293 than Myo1 and Cam1, but prior to budding off, where, like CAPZA<sup>Acp1</sup>, Sla2 and  
294 actin, it remains associated with laterally oscillating internalised endosomes  
295 (Figure 5B-C). Similarly, simultaneous imaging of Cam1 and Cam2 in  
296 *cam1.mCherry cam2.gfp* cells revealed each protein localises to many foci

297 lacking the other calmodulin, indicating differences in the timing of endocytic  
298 recruitment (Figure 5D). While Cam1 recruitment to endocytic foci is abolished  
299 in the absence of Myo1 (Figure 5E), the intensity, volume and number of Cam2  
300 foci increases in the absence of Myo1 (Figure 5F Table 1). However,  
301 internalisation and lateral “oscillating” dynamics of Cam2, and actin were  
302 dependent on Myo1 (Figure 5F & G). Therefore, while Cam1 and Cam2 both  
303 localise to sites of endocytosis, they appear to do so at different times, and each  
304 have differing Myo1 dependencies.

305 TIRF analysis revealed on average a total of ~30 Cam2 molecules recruit to  
306 each endocytic foci, and the kinetics of its recruitment to foci differ significantly  
307 to that observed for both Myo1 and Cam1. Cam2 often had a linear binding  
308 relationship (Figure 6A), which contrasts to the sigmoidal profiles observed for  
309 Myo1 and Cam1 (Figure 3C & E). TIRFM confirmed Cam2 remained associated  
310 with endocytic vesicles after they were internalised and their connection with  
311 the cell membrane was broken (Movie 3). Background corrected intensity  
312 traces of Cam2 dynamics at the membrane patch before, during, and after the  
313 end of endocytosis showed the signal rapidly dropped to baseline (<1s) (Figure  
314 6A), with the Cam2 labelled vesicles remaining visible close to the membrane  
315 at the limit of the evanescent field. A large number of these mobile internalised  
316 Cam2 labelled vesicles were seen moving within the cytoplasm with relatively  
317 low cytosolic background signal (Movie 3), indicating much Cam2 associates  
318 with endocytic vesicles and remains bound to mature endosomes. During the  
319 latter stages of endocytosis, Cam2 was internalised on the endosome while  
320 Myo1 remained at the plasma membrane during endosome abscission (Sirotkin  
321 *et al*, 2010; Berro & Pollard, 2014; Picco *et al*, 2015). Timing of the Myo1 and  
322 Cam2 fluorescence signals did not correlate; Cam2 was associated with the  
323 endocytic vesicle moving away from the cell surface during endocytosis and  
324 remaining associated with the early endosome at the time of scission. Whereas,  
325 Myo1 and Cam1 remained immobile and stayed close to the cell surface  
326 (plasma membrane) throughout the endocytic cycle.

327 To correlate Myo1-Cam1 association at sites of endocytosis with scission of the  
328 endosome into the cytoplasm, we followed Cam1 and Cam2 dynamics  
329 simultaneously in *cam1.mCherry cam2.gfp* cells (Movie 4). An average curve

330 generated from profiles of >30 complete individual endocytic events (Figure 6B)  
331 shows Cam2 moves away from the cell surface shortly after Cam1 leaves but  
332 before Myo1, with the time of abscission ( $T_{scis}$ ) occurring on average 13.4 sec  
333 after the event starts ( $T_{start}$ ). Therefore endosome scission takes place during  
334 the Myo1 disassembly phase, and around the time Cam1 dissociates from  
335 Myo1.

336 Intriguingly, while the overall distribution of Myo1 and Cam1 appeared  
337 unaffected in *cam2* $\Delta$  cells, the number, volume and intensity of foci were  
338 significantly reduced (Figure 6C-D Table 1). TIRF-based analysis of the spatial  
339 distribution of Myo1 and Cam1 at endocytic foci revealed that Cam1 organised  
340 into more dispersed foci in the absence of Cam2 (Figure 6E-F), indicating Cam2  
341 plays a role in organising the Myo1-Cam1 complex at the plasma membrane.

342

343 **Serine 742 phosphorylation increases the affinity of a single Cam2 for**  
344 **Myo1.**

345 *In vitro* analysis revealed two Cam2 molecules can associate with the  
346 unphosphorylated Myo1<sup>IQ12</sup> region (Figure 6G) with 2 distinct phases. In  
347 contrast to Cam1 binding, 70% of the signal change is associated with an  
348 affinity of 1.10  $\mu$ M. The smaller tighter signal change is not accurately  
349 measurable, but the combined change in signal is consistent with 2 binding  
350 events. As predicted from sequence analysis, Cam2 was not seen to associate  
351 with calcium (Figure 2D), and its conformation and interactions with Myo1 were  
352 insensitive to the divalent cation (Figure 6H). Like Cam1, Cam2 had a higher  
353 affinity for the first IQ motif (0.4  $\mu$ M) than both IQ12 together, and did not bind  
354 to IQ2 alone (Figure 2J). Cam1 calcium binding, as measured by IAANS  
355 labelling or change in Quin-2 fluorescence were unaffected by Cam2, while gel  
356 filtration and fluorescence binding assays provided no evidence of a direct  
357 physical interaction between the two proteins (Figure S4). Interestingly a  
358 difference was observed in fluorescence amplitudes between Cam1 and Cam2  
359 binding to the IQ12 motif, may indicate an impact upon lever arm length, (Figure  
360 6H), potentially providing a mechanism to directly control Myo1 motor activity.  
361 Myo1<sup>S742</sup> phosphorylation had no measurable impact upon the dynamics and

362 distribution of Cam2 within fission yeast cells undergoing normal vegetative  
363 growth (Figure 7A Table 1). In contrast, *in vitro* analysis revealed Cam2 was  
364 only able to occupy one of the two IQ motifs in the Myo1<sup>S742D-IQ12</sup> protein, be  
365 that with an increased affinity to the unphosphorylated protein (0.25  $\mu$ M) (Figure  
366 6G), indicating Cam2 impacts Myo1 function outside of the vegetative life cycle.

367

### 368 **Cam1 and Cam2 associate with Myo1 during meiosis.**

369 Calcium levels within log phase yeast cells are relatively low (100-200 nM) (Ma  
370 *et al*, 2011; Miseta *et al*, 1999), and provides favourable conditions for Cam1 to  
371 associate with Myo1 (pCa - 5.87). Analysis of cell fluorescence indicated the  
372 relative abundance of Myo1 : Cam1 : Cam2 within the *S. pombe* cell to be 0.2  
373 : 1.45 : 1 (Table 1), which is similar to the ratios defined by quantitative  
374 proteomic analysis of 0.45 : 1.56 : 1 (Marguerat *et al*, 2012). Similarly, image  
375 analysis of Cam1-GFP fluorescence revealed 1.7% of Cam1 to be associated  
376 with discrete foci within cells (Table 1), 40% of which is dependent upon Myo1,  
377 with the majority associating with the SPB (Figure 5D). This indicates ~0.68%  
378 of cellular Cam1 associates with Myo1 at dynamic endocytic foci. These relative  
379 protein levels, binding affinities and low Ca<sup>2+</sup> concentrations favour Cam1  
380 binding to Myo1, over Cam2 at both IQ sites (Figure 7B), consistent with *in vivo*  
381 observations.

382 While Ca<sup>2+</sup> levels are low during vegetative growth, sporadic prolonged calcium  
383 bursts occur upon pheromone release during mating (Carbó *et al*, 2016; Iida *et al*,  
384 1990), and levels elevate significantly (~10 fold) during the subsequent  
385 meiosis and sporulation (Suizu *et al*, 1995). Cam1 would be less likely to bind  
386 to Myo1 in these conditions (pCa 5.87). Myo1<sup>S742</sup> is phosphorylated from G1,  
387 through cell fusion, persisting until completion of spore formation (Figure 7C).  
388 In addition Cam2 abundance increases significantly in relation to Cam1 during  
389 G1 upon mating and entry into meiosis (Mata & Bähler, 2006; Mata *et al*, 2002).  
390 These provide conditions that would favour Myo1-Cam2 interactions over  
391 Cam1 (Figure 7B), which is consistent with both Myo1 and Cam2 playing  
392 important role at the leading edge of forespore membrane formation during  
393 meiosis (Toya *et al*, 2001; Itadani *et al*, 2007). Consistent with this prediction,

394 Myo1, Cam1, Cam2 foci lifetime and dynamics differ significantly to those  
395 observed in vegetative cells ( $P < 0.0001$ ), lasting significantly longer ( $> 1$  min) in  
396 meiotic and sporulating cells (Figure 7D & E). In contrast to vegetative cells,  
397 during meiosis and subsequent spore formation, like Myo1 and Cam1, Cam2  
398 and actin foci were less dynamic, lacking any oscillation and remain in a fixed  
399 position with significantly longer lifetime than within actively growing cells  
400 (Figure 7D, Movie 5-8).

401 Finally, we used the *myo1.S742A* allele to explore the impact of Myo1<sup>S742</sup>  
402 phosphorylation on Myo1, Cam1 and Cam2 dynamics and function during  
403 meiosis. In contrast to wild type, the lifetime of Cam1 foci were significantly  
404 shorter in *myo1.S742A* cells, and did not correlate with Myo1 and Cam2  
405 dynamics, both of which differed significantly from *myo1*<sup>+</sup> cells (Figure 7F). The  
406 majority of Cam2 foci remained present in the cell for greater than 2 mins in  
407 meiotic cells lacking Myo1<sup>S742</sup> phosphorylation, which also differed significantly  
408 from Myo1<sup>S742A</sup> dynamics, indicating normal Cam1 and Cam2 interactions with  
409 Myo1 were abolished. Consistent with *myo1.S742A* cells grown to stationary  
410 phase in minimal media (Figure 1F), heterothallic (*h*<sup>90</sup>) G1 arrested nitrogen  
411 starved *myo1.S742A* cells failed to inhibit polar growth (Figure 7G), mating cells  
412 accumulated with abnormal shmoo tips, and meiosis often resulted in cells with  
413 too few unequally sized spores (Figure 7G arrowheads). This spore defect  
414 phenotype is similar to that observed in *cam2Δ* cells (Itadani *et al*, 2007), which  
415 is consistent with a model whereby increase in cellular Ca<sup>2+</sup> and Myo1<sup>S742</sup>  
416 phosphorylation are both key for Cam2 association with and regulation of Myo1.

417 These data support a model by which changes in calcium levels and TORC2  
418 dependent phosphorylation status provide a simple two stage mechanism for  
419 modulating motor activity by modifying lever arm length as well as switching  
420 calmodulin light chain preference to regulate myosin function in response to  
421 changing needs of the cell (Figure 7B).

## 422 Discussion

423 Myosins are subject to diverse systems of regulation, which include  
424 composition of the actin track, cargo and light chain interactions, as well as  
425 phosphorylation. Here we describe a newly discovered mechanism by which  
426 phosphorylation of the myosin heavy chain (Figure 1) regulates light chain  
427 specificity, lever arm conformation and flexibility, to modulate and control  
428 cellular function. During the vegetative life cycle, within basal levels of cellular  
429 calcium, the fission yeast myosin-1 preferentially associates with two molecules  
430 of the calcium regulated calmodulin light chain Cam1 (Figures 2 & 3). During  
431 early stages of the cell cycle TORC2 dependent phosphorylation of the Myo1  
432 neck region, to which the light chain(s) bind, changes the length of the Cam1  
433 associated lever arm to moderate its activity to regulate the rate of endocytosis  
434 (Figure 4).

435 During the sexual cycle, Myo1<sup>S742</sup> remains phosphorylated (Figure 7). This  
436 combined with the increase in cytosolic Ca<sup>2+</sup> levels leads to a switch in light  
437 chain preference to a single molecule of the calcium insensitive calmodulin like,  
438 Cam2. The single Cam2 molecule is likely to bind IQ1 of S742 phosphorylated  
439 Myo1, as comparison with the structure of the IQ region of Myosin-1 and  
440 calmodulin (Lu *et al*, 2014), phosphorylation of S742 is likely to impact  
441 calmodulin interactions at the 1<sup>st</sup> IQ position. Furthermore, our data reveals that  
442 Cam2 is unable to associate with IQ2 alone, as it is necessary for one  
443 calmodulin to occupy IQ1 in order for a second to bind to IQ2. This switch in  
444 light chain occupancy may provide a mechanism to change the stiffness of the  
445 Myo1 neck region (i.e. the “lever arm”) and thereby modulate the movement  
446 and force it produces during the acto-myosin ATPase cycle and/or the load-  
447 sensitivity of its actin-bound lifetime.

448 While Myo1 is capable of associating with phospholipid membranes via its  
449 Plekstrin Homology (PH) domain, *in vivo* data suggests that this alone is not  
450 sufficient to enable a stable interaction at the plasma membrane (Figure 8A).  
451 The build-up of the early endocytic markers, such as Pan1 or Sla1, are  
452 necessary to catalyse its nucleation to early endocytic patches allowing Myo1  
453 foci to form at the site of membrane invagination. This is consistent with our  
454 observation that once initiated, Myo1-Cam1 foci do not collapse, but go on to

455 complete the endocytic event (**Figure 8B**) (Sun *et al*, 2015; Barker *et al*, 2007).  
456 Similarly, the size of this early marker “patch” has a direct impact upon the  
457 number of Myo1 molecules recruited to the plasma membrane, which is  
458 consistent with the role of Pan1 in enhancing the Arp2/3 actin nucleating activity  
459 of myosin-1 foci in yeast (Barker *et al*, 2007).

460 The local concentration of Myo1 at the endocytic patch appears critical, rather  
461 than the absolute number of Myo1 molecules, as the latter does not affect the  
462 duration of the Myo1 driven event. Indeed the duration of Myo1’s residency at  
463 the plasma membrane is driven by Cam1 and phosphorylation regulated neck  
464 length. Interestingly neither of these factors affect the rate of Myo1 or Cam1  
465 recruitment or disassociation from the membrane.

466 Therefore the size of the Pan1 patch determines the number of Myo1 molecules  
467 necessary to generate a critical local concentration of Arp2/3 nucleated actin  
468 filaments (**Figure 8C**) (Barker *et al*, 2007). At the critical concentration myosin  
469 heads are able to interact with actin filaments nucleated from either adjacent  
470 Myo1 tails or WASP activated Arp2/3 complexes, tethered to the membrane via  
471 molecules such as the Talin like Sla2 (**Figure 8D**) (Sirotkin *et al*, 2005; 2010).  
472 The Myo1 is then primed to act as a tension sensor against the actin filament,  
473 as it pushes against the membrane of the internalised endosome, which grows  
474 against the significant 0.85 MPa (8.3 atm) turgor pressure within the cell (Minc  
475 *et al*, 2009) (**Figure 8E**). While observations within budding yeast indicate motor  
476 activity from a ring of myosins at the lip of the endosome (Mund *et al*, 2018) is  
477 necessary for endocytic internalisation the mechanism by which the myosin  
478 interacts with actin to facilitate this is unknown (Sun *et al*, 2006).

479 The number of Myo1 molecules at the plasma membrane foci remains constant,  
480 as the membrane is internalised, until 2 seconds after Cam1 disassociates from  
481 Myo1 (**Figure 8F**). While the trigger for Cam1 release is unknown, the rapid  
482 ensemble nature of the event indicates it is likely to be initiated by a rapid  
483 localised spike in calcium. This could perhaps be driven by a critical level of  
484 membrane deformation coupled to calcium influx - similar to processes  
485 proposed for mechano-transduction and the role of mammalian myosin-1 within  
486 the stereocilia of the inner ear (Adamek *et al*, 2008; Batters *et al*, 2004).  
487 Alternatively, mechanical forces acting on Myo1 may drive Cam1 dissociation.



488 Genetics studies from budding yeast indicate that calmodulin mutants, unable  
489 to bind  $\text{Ca}^{2+}$ , release normally from myosin-1 (Geiser *et al*, 1991). Research  
490 using mammalian brush border myosin-1, indicates that changes in lipid  
491 composition of membranes to which the motor is associated are sufficient to  
492 displace calmodulin from the IQ region (Hayden *et al*, 1990). In fission yeast  
493 this change in lipid could be rapidly triggered by PI4-kinase phosphorylation  
494 (Cam2 is the light chain for PI4 kinase (Sammons *et al*, 2011)). This is  
495 consistent with timing of Cam2 membrane recruitment and could go some way  
496 to explain why Myo1 foci are more dispersed in absence of Cam2.

497 Once Cam1 detaches from the Myo1 molecule, the neck loses rigidity (Figure  
498 8F), reducing tension between the myosin motor and actin filament, causing it  
499 to detach rapidly from F-actin (Lewis *et al*, 2012; Menten *et al*, 2018). Given  
500 the off-rate of single Myo1 molecules from the plasma membrane is  $\sim 2 \text{ sec}^{-1}$   
501 (Figure 3B), lack of association with actin would mean that Myo1 would leave  
502 the endocytic patch a second or so after losing its Cam1 light chain. Together  
503 these events account for the 2 sec delay between disappearance of Cam1 and  
504 Myo1 from the membrane. The same drop in tension at the plasma membrane  
505 could provide the signal for scission of the endosome (Palmer *et al*, 2015).

506 The conformation and rigidity of the Myo1 lever arm would therefore play a key  
507 role in modulating the tension sensing properties of the motor domain. This is  
508 consistent with our data, where wild type phosphorylatable Myo1 resides at the  
509 membrane  $\sim 1.8 \text{ sec}$  longer than unphosphorylated Myo1<sup>S742A</sup> (Figure S2).  
510 Phosphorylation-dependent changes in the conformation of the myosin neck  
511 provide a simple mechanism to modulate the rate of endocytosis according to  
512 the size and needs of the cell. Similarly, in the presence of  $\text{Ca}^{2+}$  and Myo1<sup>S742</sup>  
513 phosphorylation, a single Cam2 resides at IQ1 motif of the neck (Figure 7B),  
514 again modulating neck conformation adjacent the motor domain as well as  
515 allowing flexibility within the carboxyl half of the neck region. This would provide  
516 a relatively tension insensitive motor, that stalls against the actin polymer, and  
517 would therefore persist significantly longer at the endocytic foci, as observed  
518 here (Figure 7E). These changes in lever arm properties change the overall  
519 rate of endocytosis, as observed in differences for actin labelled endosomes to  
520 internalise (Figure 4A).

521 Thus phosphorylation-dependent changes in the calcium regulated  
522 conformation and rigidity of the myosin lever arm could provide a universal  
523 mechanism for regulating the diverse cytoplasmic activities and functions of  
524 myosin motors within all cells.

525

## 526 **Materials and Methods**

527 **Yeast cell culture:** Cell culture and maintenance were carried out according to  
528 (Moreno *et al*, 1991) using Edinburgh minimal medium with Glutamic acid  
529 nitrogen source (EMMG) unless specified otherwise. Cells were cultured at 25  
530 °C unless stated otherwise and cells were maintained as early to mid-log phase  
531 cultures for 48 hours before being used for analyses. Genetic crosses were  
532 undertaken on MSA plates (Egel *et al*, 1994). All strains used in this study were  
533 prototroph and listed in Supplementary Table 1.

534 **Molecular Biology:** *cam1*<sup>+</sup> (SPAC3A12.14), *cam1.T6C* and *cam2*<sup>+</sup>  
535 (SPAC29A4.05) genes were amplified as *Nde1* - *BamH1* fragments from  
536 genomic *S. pombe* DNA using o226/o227 and o393/o394 primers and cloned  
537 into pGEM-T-Easy (*Promega*, Madison, WI, USA). After sequencing the  
538 subsequent genes were cloned into pJC20 (Clos *et al.*, 1990) to generate  
539 bacterial calmodulin expression constructs. DNA encoding for the FRET  
540 optimized fluorophores CyPet and YPet (Nguyen and Daugherty, 2005) were  
541 each amplified using primers o405 / o406 and o403 / o404 respectively. o406  
542 also incorporated DNA at the 3' end of the CyPet ORF encoding for the first IQ  
543 motif of the Myo1 neck region, while o404 included DNA encoding a Gly3His6  
544 tag at the 3' of the YPet ORF. The two DNA fragments were cloned into pGEM-  
545 T-Easy in a three-way ligation reaction to generate pGEM-CyPet-Myo1<sup>IQ1</sup>-  
546 YPet. The CyPet-Myo1<sup>IQ1</sup>-YPet DNA was subsequently sequencing and cloned  
547 as a *Nde1* - *BamH1* fragment into pJC20 (Clos & Brandau, 1994) to generate  
548 pJC20CyPet-Myo1<sup>IQ1</sup>-YPet. Complementary oligonucleotides o425 & o426  
549 were annealed together and ligated into *BglII* – *Xho1* cut pJC20CyPet-Myo1<sup>IQ1</sup>-  
550 YPet to generate pJC20CyPet-Myo1<sup>IQ12</sup>-YPet. Similarly, complementary  
551 oligonucleotides o429 & o430 were annealed together and subsequently  
552 ligated into *Sal1*-*BglII* cut pJC20CyPet-Myo1<sup>IQ1</sup>-YPet and the subsequent *Xho1*  
553 fragment was excised to generate pJC20CyPet-Myo1<sup>IQ2</sup>-YPet. Site directed  
554 mutagenesis was carried out using pJC20CyPet-Myo1<sup>IQ12</sup>-YPet template and  
555 o427 & o428 primers to generate pJC20CyPet-Myo1<sup>IQ12</sup>S742D-YPet.  
556 Complementary oligonucleotides o449 & o450 were annealed together and  
557 ligated into *Nru1* – *Xho1* digested pJC20CyPet-Myo1<sup>IQ12</sup>S742D-YPet to  
558 generate pJC20CyPet-Myo1<sup>IQ12</sup>S742A-YPet. All plasmids were sequenced

559 upon construction. Strains with fluorophore tagged alleles of *cam1*<sup>+</sup> and *cam2*<sup>+</sup>  
560 were generated as described previously using appropriate template and  
561 primers (Bähler *et al*, 1998). Strains in which the *myo1.S742A*, *myo1.S742D*,  
562 *mNeongreen-myo1*, *mNeongreen-myo1.S742A*, or *mNeongreen-myo1.S742D*  
563 alleles replaced the endogenous *myo1*<sup>+</sup> gene (SPBC146.13c) were generated  
564 using a marker switching method (Maclver *et al*, 2003). Oligonucleotides are  
565 described in Supplementary Table 2.

566 **Protein expression & purification:** All recombinant proteins were expressed  
567 and purified from BL21 DE3 *E. coli* cells, except Cam1 proteins where BL21  
568 DE3 pNatA cells (Eastwood *et al*, 2017) were used to allow amino-terminal  
569 acetylation (Figure S1). **Calmodulin purification:** Cell lysates were resuspended  
570 in Buffer A (50 mM Tris, 2 mM EDTA, 1 mM DTT, 0.1 mM PMSF, pH 7.5) and  
571 precleared by high speed centrifugation (48,500 RCF; 30 min; 4 °C), before  
572 ammonium sulphate was added to the supernatant at 35 % saturation,  
573 incubated for 30 minutes at 4 °C. Precipitated proteins were removed by  
574 centrifugation (48,500 RCF; 30 min; 4 °C). For Cam1 purifications the  
575 precipitation cleared supernatant was added to a pre-equilibrated 10 ml phenyl  
576 sepharose (CL-4B) column (Buffer B: 50 mM Tris, 1 mM DTT, 1 mM NaN<sub>3</sub>, 5  
577 mM CaCl<sub>2</sub>, pH 8.0), washed in 4 volumes of Buffer B before eluted as fractions  
578 in Buffer C (50 mM Tris, 1 mM DTT, 1 mM NaN<sub>3</sub>, 5 mM EGTA, pH 8.0). For  
579 Cam2 purification the precipitation cleared supernatant underwent a second  
580 round of ammonium sulphate precipitation and clearing, and the subsequent  
581 supernatant subjected to isoelectric precipitation (pH 4.3) and centrifugation  
582 (48,500 RCF: 30 minutes; 4 °C). The resultant pellet was resuspended in Buffer  
583 A, heated to 80 °C for 5 minutes and denatured proteins removed by  
584 centrifugation (16,000 RCF; 5 min). *His-tagged* proteins were purified in native  
585 conditions using prepacked, pre-equilibrated 5ml Ni<sup>2+</sup> columns.

586 **Fast reaction kinetics:** All transient kinetics were carried out using a HiTech  
587 Scientific DF-61 DX2 Stopped Flow apparatus (TgK Scientific, Bradford-upon-  
588 Avon, UK) at 20°C. All data was acquired as the average of 3-5 consecutive  
589 shots and analysed using the KineticStudio software supplied with the  
590 equipment. Quin-2 fluorescence was excited at 333 nm and used a Schott  
591 GG445 cut off filter to monitor fluorescence above 445 nm. IAANS (2-(4'-

592 (iodoacetamido)anilino)-naphthalene-6-sulfonic acid) was excited at 335 nm  
593 and fluorescence was monitored through a GG455 filter. For the FRET  
594 measurements, CyPet was excited at 435 nm and YPet emission was  
595 monitored through a combination of a Wrattan Gelatin No12 (Kodak) with a  
596 Schott GG495 nm filter to monitor fluorescence at 525-530 nm.

597 **Fluorescence spectra:** Emission spectra were obtained using a Varian Cary  
598 Eclipse Fluorescence Spectrophotometer (Agilent Technologies, Santa Clara,  
599 CA) using a 100  $\mu$ l Quartz cuvette. For FRET measurements samples were  
600 excited at 435 nm (CyPet excitation) and emission was monitored from 450 –  
601 600 nm with both slits set to 1 nm. Affinity experiments were carried out using  
602 1  $\mu$ M IQ-FRET protein with varying concentrations of Cam1 or Cam2 in a final  
603 volume of 100  $\mu$ l in analysis buffer of 140 mM KCl, 20 mM MOPS, pH 7.0 with  
604 or without 2 mM MgCl<sub>2</sub> and with 2 mM of EGTA, CaCl<sub>2</sub> or Ca<sup>2+</sup>-EGTA as  
605 required.

606 **Live cell imaging:** Live cell widefield fluorescence imaging was undertaken as  
607 described previously (Baker *et al*, 2016). For Total Internal Reflection  
608 Fluorescence Microscopy (TIRFM) *S. pombe* cells were immobilized on No1,  $\emptyset$   
609 25 mm lectin coated coverslips and placed into imaging chambers filled with  
610 EMMG medium. A previously described custom TIRF Microscope (Mashanov  
611 *et al*, 2003) was used to image individual cells at a rate of 20 fps in either single  
612 or dual colour mode. Lasers: 488 nm/100 mW and 561 nm/150 mW (*Omicron*,  
613 Germany); emission filters 525/50 nm and 585/29 nm, dichroic mirror 552 nm  
614 (*Semrock*, NY); all lenses and mirrors (*Thorlabs*, NJ), except two  $\emptyset$  3 mm  
615 mirrors (*Comar Optics*, UK) which directed light in and out of the 100 $\times$  1.45 NA  
616 objective lens (*Olympus*, Japan). Sequences of images were captured using  
617 one or two iXon897BV cameras (*Andor Technology*, UK) with custom made  
618 acquisition software. 100% laser power (488 nm) was used to image individual  
619 mNeogreen-Myo1 and Cam1-GFP molecules. The laser intensity was  
620 reduced to  $\leq$  20% during endocytosis imaging experiments to minimize  
621 photobleaching. All imaging was undertaken at 23 °C.

622 **Image analysis:** *Widefield data* was analysed using Autoquant software  
623 (*MediaCybernetics*, Rockville, MD, USA). All 3d image stacks were subjected  
624 to blind 3d deconvolution before analysis. Average size and number and

625 cellular distribution of foci were calculated from all foci present within  $\geq 30$  cells  
626 for each sample examined. Timing of foci events were calculated from  
627 kymographs generated in Metamorph software (*Molecular Devices*, Sunnyvale,  
628 CA, USA). The proportion of cells displaying a bent cell phenotype was  
629 determined from more than  $>350$  calcofluor ( $1 \text{ mg.ml}^{-1}$ ) stained cells for each  
630 strain. Bent cells were defined by a deviation in the direction of growth of  $> 5^\circ$   
631 from the longitudinal axis. *TIRF data* analyses, including single molecule  
632 detection and tracking, was undertaken using GMimPro software (Mashanov &  
633 Molloy, 2007). Endocytic events were identified by creating an image  
634 representing the standard deviation of each pixel over the whole video  
635 sequence (known as a “z-projection”). Bright spots in this image correspond to  
636 regions of the yeast cell that showed large intensity fluctuations. Regions of  
637 interest (ROIs)  $\sim 0.5 \mu\text{m}$  diameter (5x5 pixels) were created to enclose the site  
638 of endocytosis and changes in the averaged ROI intensity over the entire video  
639 record were saved for future analysis. To correct for local variation in  
640 background signal, the average intensity in a region  $1.5 \mu\text{m}$  diameter around  
641 the endocytosis site (but not including the central ROI) was subtracted. Data  
642 from ROIs that were contaminated by other endocytosis events, occurring in  
643 close proximity and close in time, were manually excluded from the analysis. It  
644 was critical to identify accurately the start and end of each endocytosis event  
645 so that individual traces could be averaged. To facilitate this, the rising and  
646 falling phases of the intensity trace were fitted with a straight line (60 data  
647 points, 3 sec duration), see **Figure 3C** for example. The intercept of this line  
648 with the baseline intensity gave the  $t_{\text{start}}$  and  $t_{\text{end}}$  values and event duration  
649 ( $T_{\text{dur}} = t_{\text{end}} - t_{\text{start}}$ ) (see **Figure 6A**). Intensity traces for each given condition were  
650 synchronised to the starting point ( $t_{\text{start}}$ ) and averaged (except Cam2-GFP  
651 traces which were synchronised using  $t_{\text{start}}$  measured from simultaneously  
652 acquired Cam1-mCherry signal). Similarly, traces were synchronised to their  
653 end point ( $t_{\text{end}}$ ) and averaged. The mean duration of the events ( $T_{\text{dur}}$ ) for each  
654 condition was then used to reconstruct the mean intensity changes with  
655 calculated errors for event amplitude and timing (**Table 2**). Since the falling and  
656 rising phases of most events fitted well to a simple linear equation, the *slope* of  
657 the fitted lines was used to estimate the rate of accumulation and dissociation  
658 of the fluorescent molecules. As Cam2-GFP remained bound to the endocytic

659 vesicle, when vesicle scission occurred intensity fell rapidly to zero as the  
660 vesicle diffused from the TIRF evanescent field; the time of scission was  
661 defined as  $t_{\text{scis}}$  (Figure 6C). Single particle tracking was performed using,  
662 GMimPro (Mashanov & Molloy, 2007) (ASPT module) so that the paths (or  
663 trajectories) of individual Myo1 molecules bound to cell membrane could be  
664 traced. Trajectories were analysed to yield mean intensities for individual  
665 NeonGreen and eGFP labelled proteins, which could be used to estimate the  
666 number of fluorescently-tagged molecules associated with each endocytotic  
667 event. Intensity-versus-time plots were generated from averages of >30 foci for  
668 each protein in each genetic background examined.

669

670

671

## 672 **Acknowledgements**

673 We thank Professors M. Balasubramanian, I. Hagan, P. Nurse, C. Shimoda and  
674 T. Pollard for strains; and Dr Ben Goult for stimulating discussions and  
675 comments on the manuscript. This work was supported by the University of  
676 Kent and funding from the Biotechnology and Biological Sciences Research  
677 Council (BB/J012793/1 & BB/M015130/1), a Royal Society Industry Fellowship  
678 to DPM; a CASE industrial bursary from Cairn Research Ltd to KB and by the  
679 Francis Crick Institute which receives core funding from Cancer Research UK  
680 (FC001119), the UK Medical Research Council (FC001119) and the Wellcome  
681 Trust (FC001119) GIM and JEM.

682

## 683 References

- 684 Adamek N, Coluccio LM & Geeves MA (2008) Calcium sensitivity of the  
685 cross-bridge cycle of Myo1c, the adaptation motor in the inner ear.  
686 *Proceedings of the National Academy of Sciences* **105**: 5710–5715
- 687 Attanapola SL, Alexander CJ & Mulvihill DP (2009) Ste20-kinase-dependent  
688 TEDS-site phosphorylation modulates the dynamic localisation and  
689 endocytic function of the fission yeast class I myosin, Myo1. *J. Cell. Sci.*  
690 **122**: 3856–3861
- 691 Baker K, Kirkham S, Hálová L, Atkin J, Franz-Wachtel M, Cobley D, Krug K,  
692 Macek B, Mulvihill DP & Petersen J (2016) TOR complex 2 localises to  
693 the cytokinetic actomyosin ring and controls the fidelity of cytokinesis. *J.*  
694 *Cell. Sci.* **129**: 2613–2624
- 695 Barker SL, Lee L, Pierce BD, Maldonado-Báez L, Drubin DG & Wendland B  
696 (2007) Interaction of the endocytic scaffold protein Pan1 with the type I  
697 myosins contributes to the late stages of endocytosis. *Molecular Biology*  
698 *of the Cell* **18**: 2893–2903
- 699 Batters C, Arthur CP, Lin A, Porter J, Geeves MA, Milligan RA, Molloy JE &  
700 Coluccio LM (2004) Myo1c is designed for the adaptation response in the  
701 inner ear. *EMBO J.* **23**: 1433–1440
- 702 Bähler J, Wu JQ, Longtine MS, Shah NG, McKenzie A, Steever AB, Wach A,  
703 Philippsen P & Pringle JR (1998) Heterologous modules for efficient and  
704 versatile PCR-based gene targeting in *Schizosaccharomyces pombe*.  
705 *Yeast* **14**: 943–951
- 706 Bement WM & Mooseker MS (1995) TEDS rule: a molecular rationale for  
707 differential regulation of myosins by phosphorylation of the heavy chain  
708 head. *Cell Motil. Cytoskeleton* **31**: 87–92
- 709 Berro J & Pollard TD (2014) Local and global analysis of endocytic patch  
710 dynamics in fission yeast using a new ‘temporal superresolution’  
711 realignment method. *Molecular Biology of the Cell* **25**: 3501–3514
- 712 Carbó N, Tarkowski N, Ipiña EP, Dawson SP & Aguilar PS (2016) Sexual  
713 pheromone modulates the frequency of cytosolic Ca<sup>2+</sup> bursts in  
714 *Saccharomyces cerevisiae*. *Molecular Biology of the Cell* **28**: 501–510
- 715 Carpy A, Krug K, Graf S, Koch A, Popic S, Hauf S & Macek B (2014) Absolute  
716 proteome and phosphoproteome dynamics during the cell cycle of  
717 *Schizosaccharomyces pombe* (Fission Yeast). *Mol. Cell Proteomics* **13**:  
718 1925–1936
- 719 Clos J & Brandau S (1994) pJC20 and pJC40--two high-copy-number vectors  
720 for T7 RNA polymerase-dependent expression of recombinant genes in  
721 *Escherichia coli*. *Protein Expression and Purification* **5**: 133–137



- 722 Crivici A & Ikura M (1995) Molecular and structural basis of target recognition  
723 by calmodulin. *Annu Rev Biophys Biomol Struct* **24**: 85–116
- 724 East DA & Mulvihill DP (2011) Regulation and function of the fission yeast  
725 myosins. *J. Cell. Sci.* **124**: 1383–1390
- 726 Eastwood TA, Baker K, Brooker HR, Frank S & Mulvihill DP (2017) An  
727 enhanced recombinant amino-terminal acetylation system and novel in  
728 vivo high-throughput screen for molecules affecting  $\alpha$ -synuclein  
729 oligomerisation. *FEBS Letters* **106**: 8157–9
- 730 Egel R, Willer M, Kjaerulff S, Davey J & Nielsen O (1994) Assessment of  
731 pheromone production and response in fission yeast by a halo test of  
732 induced sporulation. *Yeast* **10**: 1347–1354
- 733 Geiser JR, van Tuinen D, Brockerhoff SE, Neff MM & Davis TN (1991) Can  
734 calmodulin function without binding calcium? *Cell* **65**: 949–959
- 735 Hayden SM, Wolenski JS & Mooseker MS (1990) Binding of brush border  
736 myosin I to phospholipid vesicles. *J. Cell Biol.* **111**: 443–451
- 737 Heissler SM & Sellers JR (2016a) Various Themes of Myosin Regulation.  
738 *Journal of Molecular Biology* **428**: 1927–1946
- 739 Heissler SM & Sellers JR (2016b) Kinetic Adaptations of Myosins for Their  
740 Diverse Cellular Functions. *Traffic* **17**: 839–859
- 741 Iida H, Yagawa Y & Anraku Y (1990) Essential role for induced  $Ca^{2+}$  influx  
742 followed by  $[Ca^{2+}]_i$  rise in maintaining viability of yeast cells late in the  
743 mating pheromone response pathway. A study of  $[Ca^{2+}]_i$  in single  
744 *Saccharomyces cerevisiae* cells with imaging of fura-2. *J. Biol. Chem.*  
745 **265**: 13391–13399
- 746 Itadani A, Nakamura T & Shimoda C (2007) Localization of type I myosin and  
747 F-actin to the leading edge region of the forespore membrane in  
748 *Schizosaccharomyces pombe*. *Cell Struct. Funct.* **31**: 181–195
- 749 Itadani A, Nakamura T, Hirata A & Shimoda C (2010) *Schizosaccharomyces*  
750 *pombe* Calmodulin, Cam1, Plays a Crucial Role in Sporulation by  
751 Recruiting and Stabilizing the Spindle Pole Body Components  
752 Responsible for Assembly of the Forespore Membrane. *Eukaryotic Cell* **9**:  
753 1925–1935
- 754 Jacinto E, Loewith R, Schmidt A, Lin S, Rügge MA, Hall A & Hall MN (2004)  
755 Mammalian TOR complex 2 controls the actin cytoskeleton and is  
756 rapamycin insensitive. *Nat. Cell Biol.* **6**: 1122–1128
- 757 Kendrick-Jones J, Smith RC, Craig R & Citi S (1987) Polymerization of  
758 vertebrate non-muscle and smooth muscle myosins. *Journal of Molecular*  
759 *Biology* **198**: 241–252

- 760 Laplante M & Sabatini DM (2012) mTOR signaling in growth control and  
761 disease. *Cell* **149**: 274–293
- 762 Lee S, Comer FI, Sasaki A, McLeod IX, Duong Y, Okumura K, Yates JR III,  
763 Parent CA & Firtel RA (2005) TOR Complex 2 Integrates Cell Movement  
764 during Chemotaxis and Signal Relay in Dictyostelium. *Molecular Biology  
765 of the Cell* **16**: 4572–4583
- 766 Lee WL, Bezanilla M & Pollard TD (2000) Fission yeast myosin-I, Myo1p,  
767 stimulates actin assembly by Arp2/3 complex and shares functions with  
768 WASp. *The Journal of Cell Biology* **151**: 789–800
- 769 Lewis JH, Greenberg MJ, Laakso JM, Shuman H & Ostap EM (2012) Calcium  
770 regulation of Myosin-I tension sensing. *Biophysical Journal* **102**: 2799–  
771 2807
- 772 Liu L & Parent CA (2011) Review series: TOR kinase complexes and cell  
773 migration. *The Journal of Cell Biology* **194**: 815–824
- 774 Lu Q, Li J, Ye F & Zhang M (2014) Structure of myosin-1c tail bound to  
775 calmodulin provides insights into calcium-mediated conformational  
776 coupling. *Nat Struct Mol Biol* **22**: 81–88
- 777 Ma Y, Sugiura R, Koike A, Ebina H, Sio SO & Kuno T (2011) Transient  
778 Receptor Potential (TRP) and Cch1-Yam8 Channels Play Key Roles in  
779 the Regulation of Cytoplasmic Ca<sup>2+</sup> in Fission Yeast. *PLoS ONE* **6**:  
780 e22421
- 781 Maclver FH, Glover DM & Hagan IM (2003) A ‘marker switch’ approach for  
782 targeted mutagenesis of genes in *Schizosaccharomyces pombe*. *Yeast*  
783 **20**: 587–594
- 784 Marguerat S, Schmidt A, Codlin S, Chen W, Aebersold R & Bähler J (2012)  
785 Quantitative analysis of fission yeast transcriptomes and proteomes in  
786 proliferating and quiescent cells. *Cell* **151**: 671–683
- 787 Marks J & Hyams JS (1985) Localization of F-actin through the cell division  
788 cycle of *Schizosaccharomyces pombe*. *European Journal of Cell Biology*  
789 **39**: 27–32
- 790 Mashanov GI & Molloy JE (2007) Automatic detection of single fluorophores  
791 in live cells. *Biophysj* **92**: 2199–2211
- 792 Mashanov GI, Nobles M, Harmer SC, Molloy JE & Tinker A (2010) Direct  
793 observation of individual KCNQ1 potassium channels reveals their  
794 distinctive diffusive behavior. *J. Biol. Chem.* **285**: 3664–3675
- 795 Mashanov GI, Tacon D, Knight AE, Peckham M & Molloy JE (2003)  
796 Visualizing single molecules inside living cells using total internal reflection  
797 fluorescence microscopy. **29**: 142–152

- 798 Mata J & Bähler J (2006) Global roles of Ste11p, cell type, and pheromone in  
799 the control of gene expression during early sexual differentiation in fission  
800 yeast. *Proc. Natl. Acad. Sci. U.S.A.* **103**: 15517–15522
- 801 Mata J, Lyne R, Burns G & Bähler J (2002) The transcriptional program of  
802 meiosis and sporulation in fission yeast. *Nat Genet* **32**: 143–147
- 803 Menten A, Huehn A, Liu X, Zwolak A, Dominguez R, Shuman H, Ostap EM &  
804 Sindelar CV (2018) High-resolution cryo-EM structures of actin-bound  
805 myosin states reveal the mechanism of myosin force sensing.  
806 *Proceedings of the National Academy of Sciences* **115**: 1292–1297
- 807 Minc N, Boudaoud A & Chang F (2009) Mechanical forces of fission yeast  
808 growth. *Curr. Biol.* **19**: 1096–1101
- 809 Miseta A, Fu L, Kellermayer R, Buckley J & Bedwell DM (1999) The Golgi  
810 apparatus plays a significant role in the maintenance of Ca<sup>2+</sup>  
811 homeostasis in the vps33Delta vacuolar biogenesis mutant of  
812 *Saccharomyces cerevisiae*. *J. Biol. Chem.* **274**: 5939–5947
- 813 Mitchison JM & Nurse P (1985) Growth in cell length in the fission yeast  
814 *Schizosaccharomyces pombe*. *J. Cell. Sci.* **75**: 357–376
- 815 Moreno S, Klar A & Nurse P (1991) Molecular genetic analysis of fission yeast  
816 *Schizosaccharomyces pombe*. *Meth. Enzymol.* **194**: 795–823
- 817 Moser MJ, Flory MR & Davis TN (1997) Calmodulin localizes to the spindle  
818 pole body of *Schizosaccharomyces pombe* and performs an essential  
819 function in chromosome segregation. *J. Cell. Sci.* **110 ( Pt 15)**: 1805–1812
- 820 Moser MJ, Lee SY, Klevit RE & Davis TN (1995) Ca<sup>2+</sup> binding to calmodulin  
821 and its role in *Schizosaccharomyces pombe* as revealed by mutagenesis  
822 and NMR spectroscopy. *J. Biol. Chem.* **270**: 20643–20652
- 823 Mund M, van der Beek JA, Deschamps J, Dmitrieff S, Hoess P, Monster JL,  
824 Picco A, Nedelec F, Kaksonen M & Ries J (2018) Systematic Nanoscale  
825 Analysis of Endocytosis Links Efficient Vesicle Formation to Patterned  
826 Actin Nucleation. *Cell* **174**: 1–13
- 827 Nguyen AW & Daugherty PS (2005) Evolutionary optimization of fluorescent  
828 proteins for intracellular FRET. *Nat Biotechnol* **23**: 355–360
- 829 O'Connell CB, Tyska MJ & Mooseker MS (2007) Myosin at work: motor  
830 adaptations for a variety of cellular functions. *Biochim. Biophys. Acta*  
831 **1773**: 615–630
- 832 Palmer SE, Smaczynska-de Rooij II, Marklew CJ, Allwood EG, Mishra R,  
833 Johnson S, Goldberg MW & Ayscough KR (2015) A dynamin-actin  
834 interaction is required for vesicle scission during endocytosis in yeast.  
835 *Curr. Biol.* **25**: 868–878

- 836 Pasapera AM, Plotnikov SV, Fischer RS, Case LB, Egelhoff TT & Waterman  
837 CM (2015) Rac1-dependent phosphorylation and focal adhesion  
838 recruitment of myosin IIA regulates migration and mechanosensing. *Curr.*  
839 *Biol.* **25**: 175–186
- 840 Pearce LR, Komander D & Alessi DR (2010) The nuts and bolts of AGC  
841 protein kinases. *Nat Rev Mol Cell Biol* **11**: 9–22
- 842 Petersen J (2009) TOR signalling regulates mitotic commitment through  
843 stress-activated MAPK and Polo kinase in response to nutrient stress.  
844 *Biochem. Soc. Trans* **37**: 273–277 Available at:  
845 [http://eutils.ncbi.nlm.nih.gov/entrez/eutils/elink.fcgi?dbfrom=pubmed&id=1](http://eutils.ncbi.nlm.nih.gov/entrez/eutils/elink.fcgi?dbfrom=pubmed&id=19143645&retmode=ref&cmd=prlinks)  
846 [9143645&retmode=ref&cmd=prlinks](http://eutils.ncbi.nlm.nih.gov/entrez/eutils/elink.fcgi?dbfrom=pubmed&id=19143645&retmode=ref&cmd=prlinks)
- 847 Petersen J & Nurse P (2007) TOR signalling regulates mitotic commitment  
848 through the stress MAP kinase pathway and the Polo and Cdc2 kinases.  
849 *Nature Publishing Group* **9**: 1263–1272
- 850 Picco A, Mund M, Ries J, Nedelec F & Kaksonen M (2015) Visualizing the  
851 functional architecture of the endocytic machinery. *eLife* **4**:
- 852 Redowicz MJ (2001) Regulation of nonmuscle myosins by heavy chain  
853 phosphorylation. *J. Muscle Res. Cell. Motil.* **22**: 163–173
- 854 Rogers SL, Karcher RL, Roland JT, Minin AA, Steffen W & Gelfand VI (1999)  
855 Regulation of melanosome movement in the cell cycle by reversible  
856 association with myosin V. *The Journal of Cell Biology* **146**: 1265–1276
- 857 Sammons MR, James ML, Clayton JE, Sladewski TE, Sirotkin V & Lord M  
858 (2011) A calmodulin-related light chain from fission yeast that functions  
859 with myosin-I and PI 4-kinase. *J. Cell. Sci.* **124**: 2466–2477
- 860 Sirotkin V, Beltzner CC, Marchand J-B & Pollard TD (2005) Interactions of  
861 WASp, myosin-I, and verprolin with Arp2/3 complex during actin patch  
862 assembly in fission yeast. *The Journal of Cell Biology* **170**: 637–648
- 863 Sirotkin V, Berro J, Macmillan K, Zhao L & Pollard TD (2010) Quantitative  
864 analysis of the mechanism of endocytic actin patch assembly and  
865 disassembly in fission yeast. *Molecular Biology of the Cell* **21**: 2894–2904
- 866 Suizu T, Tsutsumi H, Kawado A, Suginami K, Imayasu S & Murata K (1995)  
867 Calcium ion influx during sporulation in the yeast *Saccharomyces*  
868 *cerevisiae*. *Can. J. Microbiol.* **41**: 1035–1037
- 869 Sun Y, Leong NT, Wong T & Drubin DG (2015) A Pan1/End3/Sla1 complex  
870 links Arp2/3-mediated actin assembly to sites of clathrin-mediated  
871 endocytosis. *Molecular Biology of the Cell* **26**: 3841–3856
- 872 Sun Y, Martin AC & Drubin DG (2006) Endocytic Internalization in Budding  
873 Yeast Requires Coordinated Actin Nucleation and Myosin Motor Activity.  
874 *Developmental Cell* **11**: 33–46

- 875 Takeda T & Yamamoto M (1987) Analysis and in vivo disruption of the gene  
876 coding for calmodulin in *Schizosaccharomyces pombe*. *Proc. Natl. Acad.*  
877 *Sci. U.S.A.* **84**: 3580–3584
- 878 Toya M, Motegi F, Nakano K, Mabuchi I & Yamamoto M (2001) Identification  
879 and functional analysis of the gene for type I myosin in fission yeast.  
880 *Genes Cells* **6**: 187–199
- 881 Trybus KM, Gushchin MI, Lui H, Hazelwood L, Kremmentsova EB, Volkmann N  
882 & Hanein D (2007) Effect of calcium on calmodulin bound to the IQ motifs  
883 of myosin V. *J. Biol. Chem.* **282**: 23316–23325
- 884 Tsien RY (1980) New calcium indicators and buffers with high selectivity  
885 against magnesium and protons: design, synthesis, and properties of  
886 prototype structures. *Biochemistry* **19**: 2396–2404
- 887 Wilson-Grady JT, Villén J & Gygi SP (2008) Phosphoproteome analysis of  
888 fission yeast. *J. Proteome Res.* **7**: 1088–1097
- 889 Win TZ, Mulvihill DP & Hyams JS (2002) Take five: a myosin class act in  
890 fission yeast. *Cell Motil. Cytoskeleton* **51**: 53–56
- 891
- 892

## 893 **Figure Legends**

894 **Figure 1. Myo1 serine 742 phosphorylation is TORC2 dependent.** (A) Anti-  
895 Myo1 western blot of extracts from WT, *gad8Δ*, *ste20Δ* and *myo1.S742A* cells  
896 separated using Phos-Tag SDS-PAGE reveals Myo1 is subject to multiple  
897 phosphorylation events (\*). (B) Sequence alignment of myosin IQ regions  
898 shows Myo1<sup>S742</sup> lies within an AGC consensus sequence, conserved in class I  
899 and V myosins. (C) Western blots of extracts from *myo1*<sup>+</sup> and *myo1-S742A*  
900 cells stained with Ponceau S and probed with phospho-specific anti-Myo1<sup>S742</sup>  
901 antibodies demonstrate antigen specificity. (D) Myo1<sup>S742</sup> is not phosphorylated  
902 in *ste20Δ* cells lacking the fission yeast TORC2 regulator Rictor<sup>Ste20</sup>. (E)  
903 Myo1<sup>S742</sup> is phosphorylated in cells cultured in minimal media containing  
904 Glutamic acid (EMMG) but not in EMM2 with an ammonium chloride nitrogen  
905 source. (F) WT and *myo1.S742A* cells grown to starvation in EMMG for 72 hrs.  
906 In contrast to WT, *myo1.S742A* cells fail to stop growing upon media induced  
907 G1 arrest. Scale – 5 μm.

908 **Figure 2. *In vitro* characterisation of interactions between Myo1 and**  
909 **Cam1.** (A) Predicted models of the CyPet-Cam1-YPet FRET reporter protein  
910 (Cam1-FRET) in the absence (upper panel) and presence (lower panel) of  
911 Ca<sup>2+</sup>. (B) pCa curve plotting Ca<sup>2+</sup> dependent changes of Cam1-FRET protein  
912 conformation (Δ in FRET signal). (C) pCa curve plotting Ca<sup>2+</sup> dependent  
913 changes in IAANS fluorescence of IAANS labelled Cam1-T6C. (D) Transient  
914 curves of changes in Quin2 fluorescence brought by Ca<sup>2+</sup> release from Cam1  
915 (black) and Cam2 (red). (E) Predicted models of the CyPet-Myo1<sup>IQ12</sup>-YPet  
916 FRET reporter protein (Myo1<sup>IQ12</sup>-FRET) in the absence (upper panel) or  
917 presence (lower panel) of Calmodulin binding. (F) Spectra of Myo1<sup>IQ12</sup>-FRET  
918 reporter alone (black line) or with Cam1 in the presence Ca<sup>2+</sup> (red dotted line)  
919 or absence (grey dotted line) of Ca<sup>2+</sup>. (G) Curves plotting Cam1 dependent  
920 changes of FRET donor signal of wild type (black) or S742D phosphomimetic  
921 (blue) Myo1<sup>IQ12</sup>-FRET proteins. (H) Spectra of Myo1<sup>IQ12</sup>-FRET (black traces)  
922 and Myo1<sup>IQ12-S742D</sup>-FRET (blue traces) in the absence (dashed lines) or  
923 presence (lines lines) of Cam1 illustrate differences in conformation of the Myo1  
924 neck region. (I) pCa curve plotting Ca<sup>2+</sup> dependent changes in acceptor

925 fluorescence of Myo1<sup>IQ12</sup>-FRET. (J) Curves plotting Cam1 (black) and Cam2  
926 (red) dependent changes of FRET donor signal of Myo1-FRET proteins  
927 containing single IQ domains (IQ1 – empty shapes; IQ2 – filled shapes).

928 **Figure 3. Myo1 and Cam1 dynamics in wild type and *myo1.S742A* cells.**

929 (A) Maximum projections of 31-z stack widefield images of *mNG.myo1*,  
930 *cam1.gfp* and *cam2.gfp* cells (Scales - 5  $\mu$ m). (B) An example relative intensity  
931 trace of a mNeogreen.Myo1 endocytic event. Linear fitting (60 points) was  
932 used to find the highest slope for both rising and falling edges. The intercept  
933 with zero intensity level was used to calculate  $T_{begin}$ ,  $T_{end}$ , and subsequently the  
934 duration of the event. Insert: An arrow shows the location of the endocytosis  
935 event (5X5 pixels area). (C) Averaged profile from 50 individual Myo1  
936 membrane association events described in (B), synchronised relative to  $T_{begin}$   
937 (grey line) and  $T_{end}$  (black line). (D) Plot of event duration (sec) against number  
938 of Myo1 molecules (fluorescence amplitude). (E) Averaged profile from 52  
939 individual Cam1 membrane association events from TIRFM timelapse analysis  
940 of *cam1.gfp* cells. (F) Example of fluorescence trace from simultaneously  
941 tracking Myo1 and Cam1 membrane binding and disassociation events from  
942 TIRFM timelapse analysis of *mNeogreen.myo1 cam1.mCherry* cells. (G)  
943 Averaged profiles of combined averages of individual Myo1 (black line and grey  
944 s.d.) and Myo1.S742A (grey line) membrane association events from TIRFM  
945 timelapse analysis of *mNeogreen.myo1* and *mNeogreen.myo1.S742A* cells  
946 respectively. (H) Analysis of mean duration of Myo1 and Cam1 endocytic  
947 events in wt and *myo1.S742A* cells from widefield imaging (n > 30). Asterisks  
948 denote differences with >99% confidence. (I) Analysis of mean LifeACT and  
949 Cam2 signal at endocytic foci in WT and *myo1.S742A* cells (n > 30). No  
950 differences observed at 95% level of confidence. All error bars - s.d.

951 **Figure 4. Myo1 S742 is phosphorylated in a cell cycle dependent manner**

952 **to affect polarised growth.** (A) Actin foci periodicity at ends of WT and  
953 *myo1.S742A* cells in G2 phase (n>30). Asterisks denote difference with >99%  
954 confidence. (B) Graphic highlighting Cdc10 and Cdc25 execution points in  
955 relation to cell cycle phases and periods of monopolar / bipolar growth (left).  
956 Myo1<sup>S742</sup> is phosphorylated in *cdc10.v50* arrested G<sub>1</sub> cells, but not in pre-mitotic

957  $G_2$  *cdc25.22* arrested cells (right panels). (C) Averaged growth curves from 3  
958 independent experiments of prototroph WT (empty circles) and *myo1.S742A*  
959 (grey filled circles) cells cultured in EMMG at 34 °C. Error bars - s.d. (D) Myosin-  
960 1 distribution and cell morphology of prototroph *mNeogreen.myo1<sup>+</sup>* and  
961 *mNeogreen.myo1.S742A* cells cultured in EMMG at 34 °C. Asterisks highlight  
962 long bent cells. Scale - 10  $\mu$ m. (E) Calcofluor stained WT and *myo1.S742A*  
963 cells. Asterisks highlight long bent cells displaying monopolar growth. Scale - 5  
964  $\mu$ m. (F) Ratio Sla2-mCherry fluorescence at “new”: “old” cell end, averaged  
965 from >30 growing mid-log *sla2-mCherry myo1<sup>+</sup>* (upper panel) and *sla2-mCherry*  
966 *myo1.S742A* (lower panel) cells. Boxes plot median and quartile for each length  
967 measured, lines are plotted from the mean average value at each length  
968 measured.

969 **Figure 5. Cam2 associates with internalised endocytic vesicles.** (A)  
970 Kymographs of GFP labelled foci from maximum projections of 13-z plane  
971 timelapse images of *mNeogreen.myo1* (upper panel), *cam1.gfp* (middle  
972 panel) and *cam2.gfp* (bottom panel) cells. Myo1 and Cam1 endocytic foci did  
973 not move on the membrane (black arrows). Spindle Pole Body (asterisk) and  
974 myosin V (white arrow) associated Cam1 are highlighted. In contrast Cam2 foci  
975 displayed extensive lateral movements. (B) Kymographs generated from single  
976 z-plane timelapse images of single endocytic foci surface during vesicle  
977 formation and subsequent internalisation. While Myo1 and Cam1 only  
978 associate with the plasma membrane, Cam2, Sla2 and actin are internalised  
979 on the vesicle after scission. (C) Kymographs of Cam2 and Sla2 co-  
980 internalisation in *sla2.mCherry cam2.gfp* cells. (D) Maximum projection of 31-z  
981 slice image of *cam1.mCherry cam2.gfp* cells reveals Cam1 (magenta) and  
982 Cam2 (green) colocalise to a subset of endocytic foci. (E-G) Single frames (left  
983 panels) and time kymographs (right panels) from maximum projections of 13-z  
984 plane timelapse images of *cam1.gfp* (E), *cam2.gfp* (F) and *LifeACT.mCherry*  
985 (G) in either *myo1<sup>+</sup>* (upper panels) or *myo1 $\Delta$*  (lower panels) cells show only  
986 Cam1 endocytic foci recruitment is dependent upon Myo1. Myo1 is required for  
987 internalisation of Cam2-GFP and LifeACT.mCherry labelled foci. Scales - 5  $\mu$ m.

988 **Figure 6. Cam2 impacts endosome organisation.** (A) An example of the



989 fluorescence trace of Cam2 membrane binding and vesicle internalisation  
990 event from TIRFM analysis of *cam2.gfp* cells. An abrupt drop in the  
991 fluorescence was marked as "scission time" (grey vertical line). An arrow shows  
992 the location of the monitored endocytic event (5X5 pixels area). (B) Averaged  
993 profile from 32 individual Cam2 membrane association events (green line)  
994 described in (A), together with Cam1-mCherry profile (red) from two-colour  
995 TIRFM imaging of *cam1.mCherry cam2.gfp* cells. Events were synchronized  
996 relative Cam1  $T_{\text{begin}}$ . Dashed line denotes mean timing of vesicle scission. (C)  
997 Maximum projection of 31-z slice widefield image of a mixture of prototroph  
998 *yfp.myo1 sid4.tdTomato* and *yfp.myo1 cam2Δ* cells. (D) Maximum projection of  
999 31-z slice widefield image of a mixture of prototroph *cam1.gfp sid4.tdTomato*  
1000 and *cam1.gfp cam2Δ* (arrows) cells. (E) Magnification of TIRF heat map of  
1001 endocytic Cam1 in *cam2<sup>+</sup>* (upper panel) and *cam2Δ* (lower panel) cells.  
1002 Squares correspond to regions extending outward from centre of focus. (F) Plot  
1003 of mean distribution of Cam1 across > 40 endocytic sites in WT and *cam2Δ*  
1004 cells. (G) Curves plotting Cam2 dependent changes of FRET donor signal of  
1005 wild type (black) or S742D phosphomimetic (blue) Myo1<sup>IQ12</sup>-FRET proteins. (H)  
1006 Spectra of Myo1<sup>IQ12</sup>-FRET reporter alone (black line), with Cam2 in the  
1007 presence Ca<sup>2+</sup> (grey solid line) or absence (grey dotted line) of Ca<sup>2+</sup>, or with  
1008 Cam1 in the absence of Ca<sup>2+</sup> (black dotted line). Scales – 5 μm.

1009 **Figure 7. Myo1 S742 phosphorylation regulated Cam1 and Cam2**  
1010 **dynamics during meiosis.** (A) Kymographs of Cam2.GFP foci dynamics in  
1011 *myo1<sup>+</sup>* (upper panel) and *myo1.S742A* (lower panel) cells. (B) Scheme of  
1012 consequence of phosphorylation of Myo1 Ser742 (small empty circle) and Ca<sup>2+</sup>  
1013 levels upon Cam1 (light grey filled circle) and Cam2 (dark grey filled circle)  
1014 binding to the IQ1 (solid thick black line) and IQ2 (compound line) motifs of  
1015 Myo1, and impact on relative orientation of the myosin lever arm (dashed  
1016 arrow). Highlighted combination of unphosphorylated Myo1<sup>S742</sup> & Ca<sup>2+</sup> does not  
1017 normally occur in wild type cells. (C) Western blots of extracts from G1 arrested  
1018 *cdc10.v50 myo1<sup>+</sup>*, *cdc10.v50 myo1-S742A* cells, conjugation arrested *fus1Δ*  
1019 cells or spores, probed with phospho-specific anti-Myo1<sup>S742</sup> antibodies confirm  
1020 Myo1S742 remains phosphorylated throughout the sexual cycle. (D) Maximum  
1021 projection of 13-z slice GFP fluorescence image and transmitted light image

1022 from a timelapse of vegetative (cell 1) and meiotic (cell 2) *gfp-act1* cells. Image  
1023 from a GFP-act signal. Kymographs in the right panels were generated along  
1024 the two dotted axes. (E) Histograms of lifetimes of Myo1 (black bars), Cam1  
1025 (white bars) and Cam2 (grey bars) foci in vegetative (left panel) and meiotic  
1026 (right panel) cells. (F) Lifetimes of Myo1, Cam1 and Cam2 foci in WT (white  
1027 bars) and *myo1.S742A* (black bars) meiotic cells. (G) Micrographs of  
1028 *myo1.S742A* cell morphology on starvation media. \* highlight cells with growth  
1029 and polarity defects; arrows highlight cells with elongated or abnormally bent  
1030 shmooing tips; and arrow heads highlight meioses resulting in defective spore  
1031 formation. Scales – 5  $\mu$ m.

1032 **Figure 8. Model of Myo1 tension dependent interactions at the plasma**  
1033 **membrane.** (A) Myo1 (green) transiently associates with the plasma  
1034 membrane. (B) In the presence of early markers of endocytosis (blue) this  
1035 interaction is stabilised, and Myo1 accumulates to a critical concentration at the  
1036 endocytic foci (C), whereupon myosin heads associate with growing Arp2/3  
1037 (purple) nucleated actin polymers (yellow) attached to the membrane (D), and  
1038 monitor tension between the actin filament and internalised plasma membrane  
1039 (E). Upon release of the calmodulin light chain (red), the myosin-1 would its  
1040 ability to monitor tension and subsequently disengage from the actin polymer  
1041 and membrane (F).

1042

## 1043 **Supplementary Data Legends**

### 1044 **Supplementary Figure 1. Purified proteins used during *in vitro* studies.**

1045 Coomassie stained SDS-PAGE gel of recombinant proteins expressed and  
1046 purified during this study. From left to right lanes contain (L) protein standard;  
1047 (1) Nt-acetylated Cam1; (2) Nt-acetylated Cam1-T6C; (3) Cam1-FRET; (4)  
1048 Cam2; (5) IQ12 peptide (not used during this study); (6) Myo1IQ12-FRET; and  
1049 (7) Myo1IQ12S742D-FRET.

### 1050 **Supplementary Figure 2. Relative TIRF profiles.** Combined profiles of

1051 averages from TIRFM timelapse analysis of Myo1 and Cam1 dynamics in wild  
1052 type or *myo1.S742A* strains. (A) Myo1 (blue) and Cam1 (red) membrane  
1053 association in wild type cells. (B) Myo1 membrane association in wild type  
1054 (blue) and *myo1.S742A* (red) cells. (C) Myo1 (blue) and Cam1 (red) membrane  
1055 association in *myo1.S742A* cells. (D) Cam1 membrane association in wild type  
1056 (blue) and *myo1.S742A* (red) cells.

### 1057 **Supplementary Figure 3. Myo1<sup>S742</sup> phosphorylation fluctuates in a cell 1058 cycle dependent manner.** A *cdc10.v50* culture was synchronized in G1 by

1059 shifting to 36°C for 240 min before returning to 25°C at time 0. Samples of cells  
1060 were taken every 20 minutes from the release and processed for western  
1061 blotting to monitor of Myo1<sup>S742</sup> phosphorylation (A). The membrane was  
1062 subsequently probed with anti-Myo1 antibodies (B) to monitor total Myo1. Equal  
1063 loading was monitored by Ponceau staining of the membrane. (C) Densitometry  
1064 measurements of the bands in these blots are plotted along with the % of cells  
1065 in the culture with septa.

### 1066 **Supplementary Figure 4. Cam1 and Cam2 do not interact directly.** (A)

1067 Overlaid OD280 spectra were recorded from eluate from a Superdex 75 gel  
1068 filtration column which had been loaded with either Cam1 (grey line), Cam2  
1069 (black line) or Cam1 and Cam2 (red line) under identical 4 mM EGTA buffer  
1070 conditions. (B) Maximum IAANS fluorescence values (440 nm) of 0.5 μM  
1071 Cam1-IAANS at a range of pCa values. Black symbols show values of Cam1-  
1072 IAANS, red symbols show values of Cam1-IAANS with 5 μM Cam2 protein. 2  
1073 mM Ca- EGTA buffers were used to give indicated pCa values. pCa50 values

1074 calculated from Origin fitting analysis - Hill equation.

1075 **Supplementary Figure 5. Multiple labelling strategies for Myo1, Cam1 and**  
1076 **Cam2 disrupts normal distribution.** Cam1 has increased cytoplasmic signal  
1077 and reduced signal at endocytic foci in cells expressing both *cam1.gfp* and  
1078 *mCherry.myo1* (A (GFP-green, mCherry-magenta)) compared to cells  
1079 expressing *cam1.gfp* alone (B). Similarly, Cam1 has increased cytoplasmic  
1080 signal and reduced relative signal at endocytic foci in *CFP-myo1 cam1.mCherry*  
1081 cells (C). (D) Growth curves of prototroph *cam1.gfp* (green) and *cam1.gfp*  
1082 *mCherry.myo1* cells cultured in EMMG at 25 °C. (E) Cam1 (green) localisation  
1083 is disrupted in *cam1.gfp cam2.mCherry* cells, with less Cam1 on endocytic foci,  
1084 and localising to the mitotic spindle which is never observed in cells expressing  
1085 FP labelled Cam1 alone.

1086 **Supplementary Movie 1:** Timelapse of TIRFM imaged *mNeogreen.myo1*  
1087 cells showing rapid single molecule interactions of Myo1 at the plasma  
1088 membrane. Frame Rate: 15 msec / frame.

1089 **Supplementary Movie 2:** Timelapse of TIRFM imaged *mNeogreen.myo1*  
1090 cells showing endocytosis associated interactions of Myo1 at the plasma  
1091 membrane. Frame rate: 50 msec / frame.

1092 **Supplementary Movie 3:** Timelapse of TIRFM imaged *cam2.gfp* cells showing  
1093 Cam2 recruiting to endocytic vesicles, to which it remains associated after  
1094 scission and internalisation of the endosome. Frame rate: 50 msec / frame.

1095 **Supplementary Movie 4:** Timelapse of TIRFM imaged *cam1.mCherry*  
1096 *cam2.gfp* cells showing early recruitment of Cam1 (red) subsequent  
1097 recruitment of Cam2 (green) to sites of endocytosis. Cam1 disassociates prior  
1098 to vesicle scission, while Cam2 remains associated with the internalised  
1099 endosome. Frame rate: 50 msec / frame.

1100 **Supplementary Movie 5:** Timelapse of maximum projections from 13-z slice  
1101 widefield images of *mNeogreen.myo1* cells showing typical examples of Myo1  
1102 dynamics in vegetative and meiotic cells. Frame rate: 650 msec / frame.

1103 **Supplementary Movie 6:** Timelapse of maximum projections from 13-z slice  
1104 widefield images of *cam1.gfp* cells showing typical examples of Cam1  
1105 dynamics in vegetative and meiotic cells. Frame rate: 650 msec / frame.

1106 **Supplementary Movie 7:** Timelapse of maximum projections from 13-z slice  
1107 widefield images of *cam2.gfp* cells showing typical examples of Cam2  
1108 dynamics in vegetative and meiotic cells. Frame rate: 650 msec / frame.

1109 **Supplementary Movie 8:** Timelapse of maximum projections from 13-z slice  
1110 widefield images of *gfp.act1* cells showing typical examples of Act1 dynamics  
1111 in vegetative and meiotic cells. Frame rate: 650 msec / frame.

1112 **Supplementary Table 1:** Strains used during this study.

1113 **Supplementary Table 2:** Oligonucleotides used during this study.

<b>Myo1</b>	<i>mNeonGreen-myo1</i>	<i>mNeonGreen-myo1-S742A</i>	<i>YFP-myo1 cam2Δ</i>	-
Whole cell fluorescence (AU)	9,453,813	<b>0.86</b> (0.8628)	<b>0.90</b> (0.0295)	-
Cell size (μm <sup>2</sup> )	98.9	<b>0.84</b> (0.0863)	<b>0.95</b> (0.4542)	-
Maximum intensity (AU)	33,477	<b>0.92</b> (0.1446)	<b>0.62</b> (0.0001)	-
Number of foci	15.9	<b>0.82</b> (0.0203)	<b>0.84</b> (0.0261)	-
Average foci volume (μm <sup>3</sup> )	0.98	<b>0.98</b> (0.8595)	<b>0.64</b> (0.0001)	-
Total foci volume (μm <sup>3</sup> )	15.2	<b>0.75</b> (0.0020)	<b>0.53</b> (0.0001)	-
Total foci fluorescence (AU)	139,712	<b>0.76</b> (0.0061)	<b>0.45</b> (0.0001)	-
Average foci lifetime (s)	14.0	<b>10.9</b> (0.0001)	ND	-
N =	32	30	37	-
<b>Cam1</b>	<i>cam1-gfp (myo1<sup>+</sup>)</i>	<i>cam1-gfp myo1-S742A</i>	<i>cam1-gfp cam2Δ</i>	<i>cam1-gfp myo1Δ</i>
Whole cell fluorescence (AU)	61,530,900	<b>0.89</b> (0.0197)	<b>0.97</b> (0.7145)	<b>1.14</b> (0.0733)
Cell size (μm <sup>2</sup> )	86.1	<b>0.99</b> (0.9271)	<b>1.08</b> (0.2016)	<b>1.00</b> (0.9748)
Maximum intensity (AU)	251,700	<b>0.82</b> (0.0563)	<b>0.72</b> (0.0001)	<b>1.41</b> (0.0001)
Number of foci	14.1	<b>0.96</b> (0.6960)	<b>0.93</b> (0.3200)	<b>0.42</b> (0.0001)
Average foci volume (μm <sup>3</sup> )	1.12	<b>0.67</b> (0.0081)	<b>0.74</b> (0.0321)	<b>1.52</b> (0.0188)
Total foci volume (μm <sup>3</sup> )	14.33	<b>0.68</b> (0.0004)	<b>0.78</b> (0.0703)	<b>0.56</b> (0.0001)
Total foci fluorescence (AU)	1,020,350	<b>0.63</b> (0.0002)	<b>0.66</b> (0.0013)	<b>0.60</b> (0.0001)
Average foci lifetime (s)	10.4	<b>9.4</b> (0.0001)	<b>13.3</b> (0.0001)	-
N =	25	15	56	27
<b>Cam2</b>	<i>cam2-gfp (myo1<sup>+</sup>)</i>	<i>cam2-gfp myo1-S742A</i>	-	<i>cam2-gfp myo1Δ</i>
Whole cell fluorescence (AU)	39,259,937	<b>1.01</b> (0.8063)	-	<b>1.48</b> (0.0001)
Cell size (μm <sup>2</sup> )	79.3	<b>0.89</b> (0.2385)	-	<b>1.15</b> (0.3114)
Maximum intensity (AU)	267,547	<b>0.98</b> (0.6339)	-	<b>0.78</b> (0.0001)
Number of foci	20.8	<b>0.94</b> (0.4155)	-	<b>1.26</b> (0.0048)
Average foci volume (μm <sup>3</sup> )	0.82	<b>1.11</b> (0.0737)	-	<b>1.63</b> (0.0001)
Total foci volume (μm <sup>3</sup> )	16.53	<b>1.05</b> (0.4287)	-	<b>2.10</b> (0.0001)
Total foci fluorescence (AU)	859,161	<b>1.06</b> (0.3374)	-	<b>1.82</b> (0.0001)
N =	20	31	-	17
<b>LifeAct</b>	<i>LifeAct (myo1<sup>+</sup>)</i>	<i>LifeAct myo1-S742A</i>	ND	<i>LifeAct myo1Δ</i>
Whole cell fluorescence (AU)	17,116,300	<b>1.14</b> (0.0936)	-	<b>1.15</b> (0.2851)
Cell size (μm <sup>2</sup> )	84.5	<b>1.01</b> (0.8787)	-	<b>1.14</b> (0.1529)
Maximum intensity (AU)	94,671	<b>1.06</b> (0.4403)	-	<b>0.64</b> (0.016)
Number of foci	19.8	<b>0.94</b> (0.5502)	-	<b>1.22</b> (0.0147)
Average foci volume (μm <sup>3</sup> )	0.73	<b>1.19</b> (0.0346)	-	<b>0.95</b> (0.6822)
Total foci volume (μm <sup>3</sup> )	13.96	<b>1.15</b> (0.1771)	-	<b>1.14</b> (0.2759)
Total foci fluorescence (AU)	327,017	<b>1.18</b> (0.1832)	-	<b>1.03</b> (0.8674)
N =	23	23	-	23

Table 1:

AutoQuantX3 Image analysis data of wide-field fluorescence data of cells. Mutant strains were imaged in mix experiments with wild type cells, analysis for these cells is shown relative to the wild type control cells for each experiment. Statistical significance determined by an unpaired *t*-test is shown in brackets, a statistical significance of  $p < 0.05$  is indicated in red.

Protein ( <i>myo1 allele</i> )	Duration (SEM)	Amplitude (SEM)	Rise rate (SEM)	Drop rate (SEM)	N
Myo1 ( <i>myo1</i> <sup>+</sup> )	13.84(0.39) <sup>1,2,3</sup>	2373(155)	536(40.4)	567(43)	50
Cam1 ( <i>myo1</i> <sup>+</sup> )	10.99(0.21) <sup>1</sup>	4539(292)	1074(83)	1028(69)	52
Myo1 ( <i>myo1.S742A</i> )	12.28(0.31) <sup>2,4</sup>	2274(128)	536(34)	570(41)	67
Cam1 ( <i>myo1.S742A</i> )	12.15(0.38) <sup>3,4</sup>	4629(301)	1153(98)	1031(77)	43

Significance differences observed in durations of: <sup>1</sup> Myo1 (wt cells) and Cam1 (wt cells) foci  $p < 0.0001$ ; <sup>2</sup> Myo1 (wt cells) and Myo1 (*myo1.S742A* cells) foci  $p < 0.002$ ; <sup>3</sup> Myo1 (wt cells) and Cam1 (*myo1.S742A* cells) foci  $p < 0.0064$ .

<sup>4</sup> No significant difference observed between duration of Myo1 (*myo1.S742A* cells) and Cam1 (*myo1.S742A* cells) foci  $p < 0.79$ .

Table 2:

Image analysis data of TIRF data of cells of the indicated genotype.

Figure 1

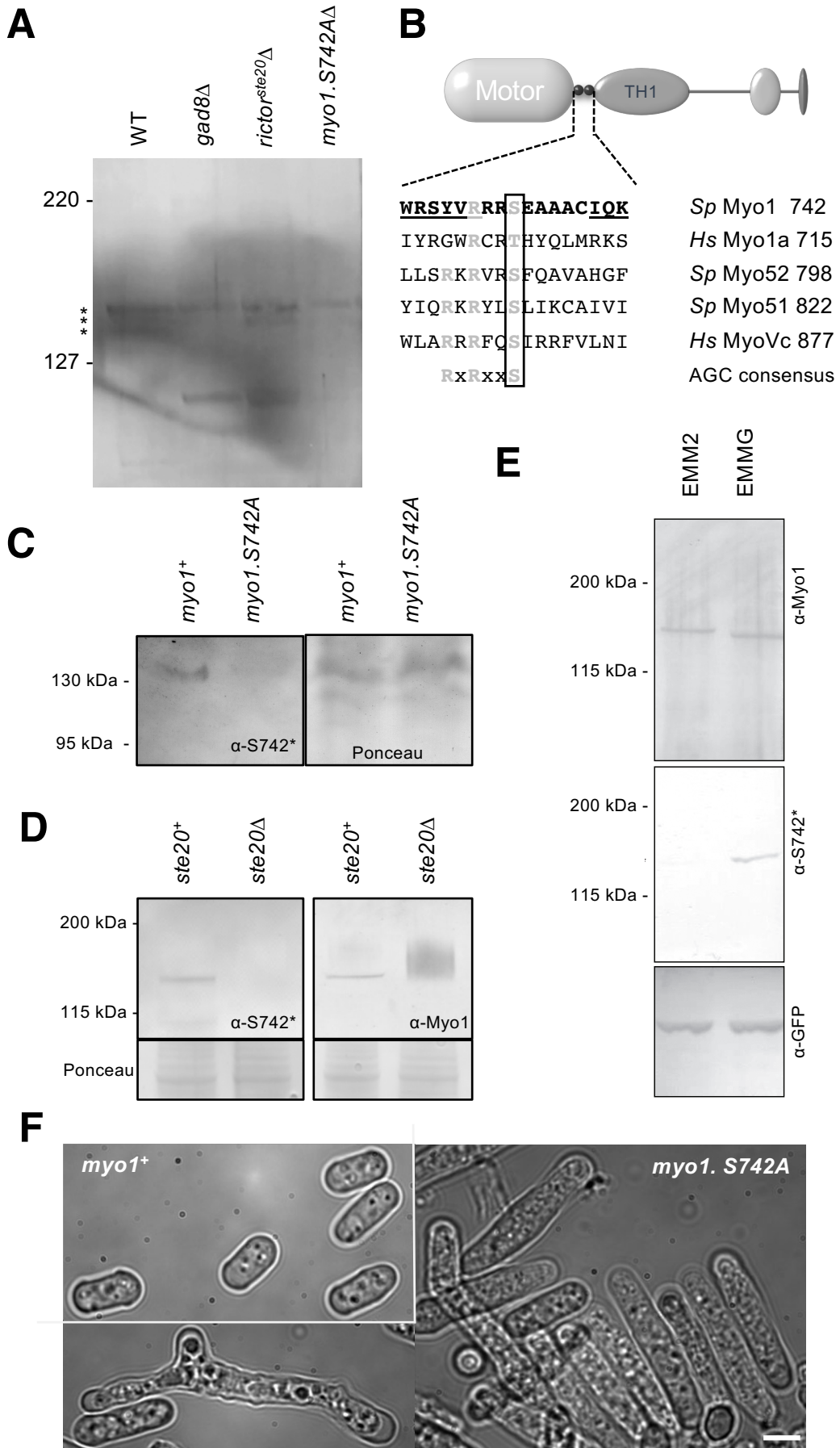




Figure 2

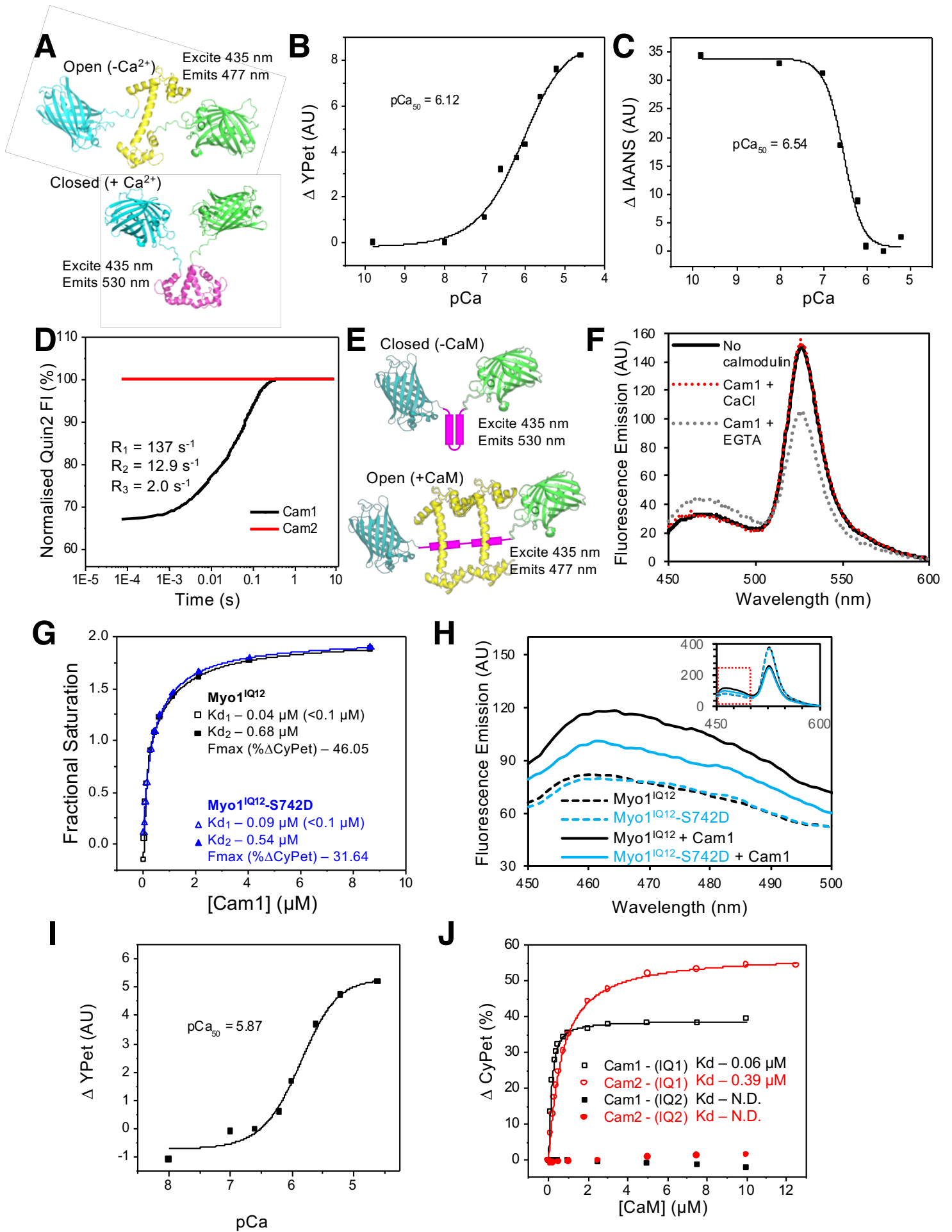


Figure 3

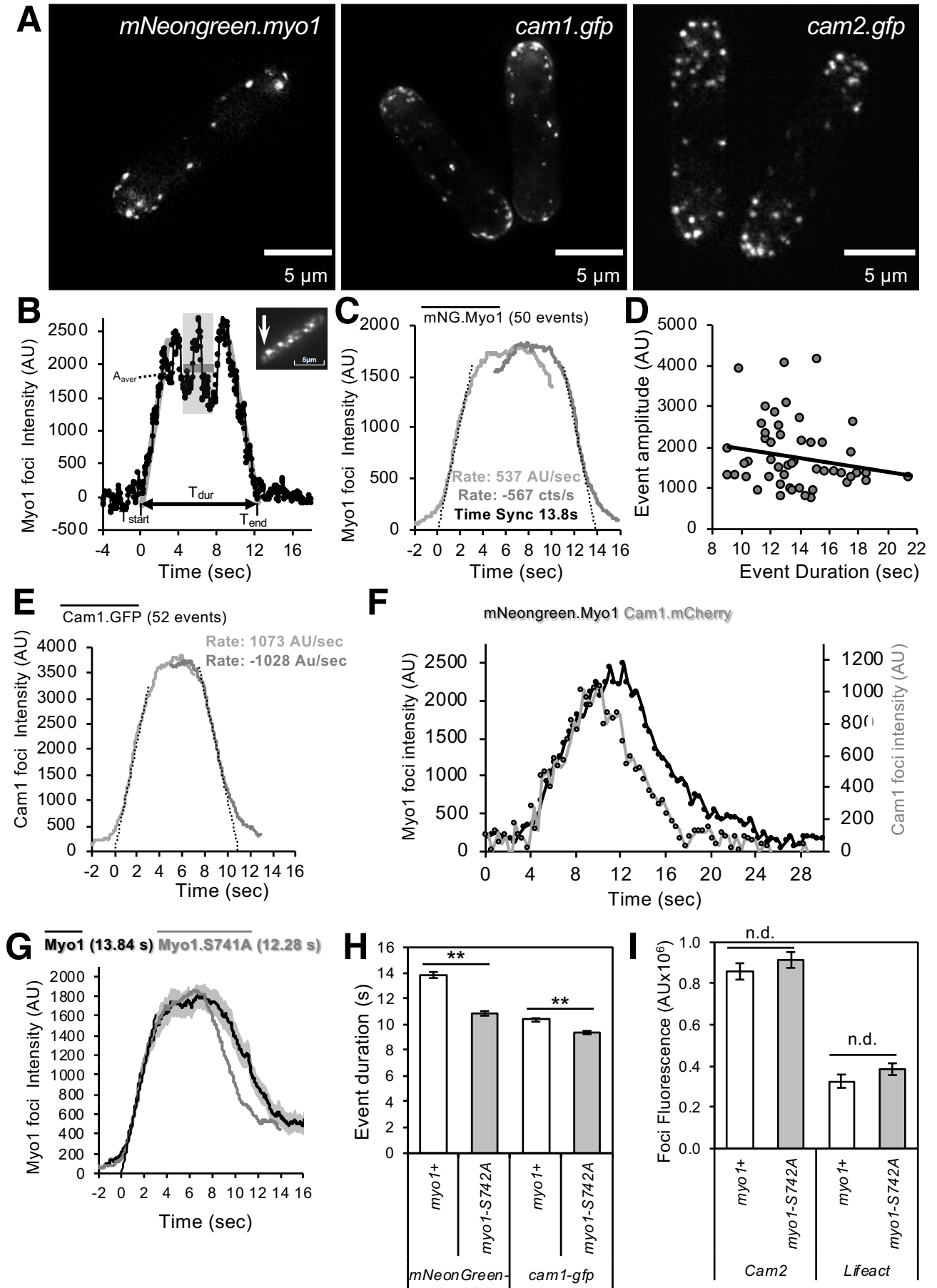


Figure 4

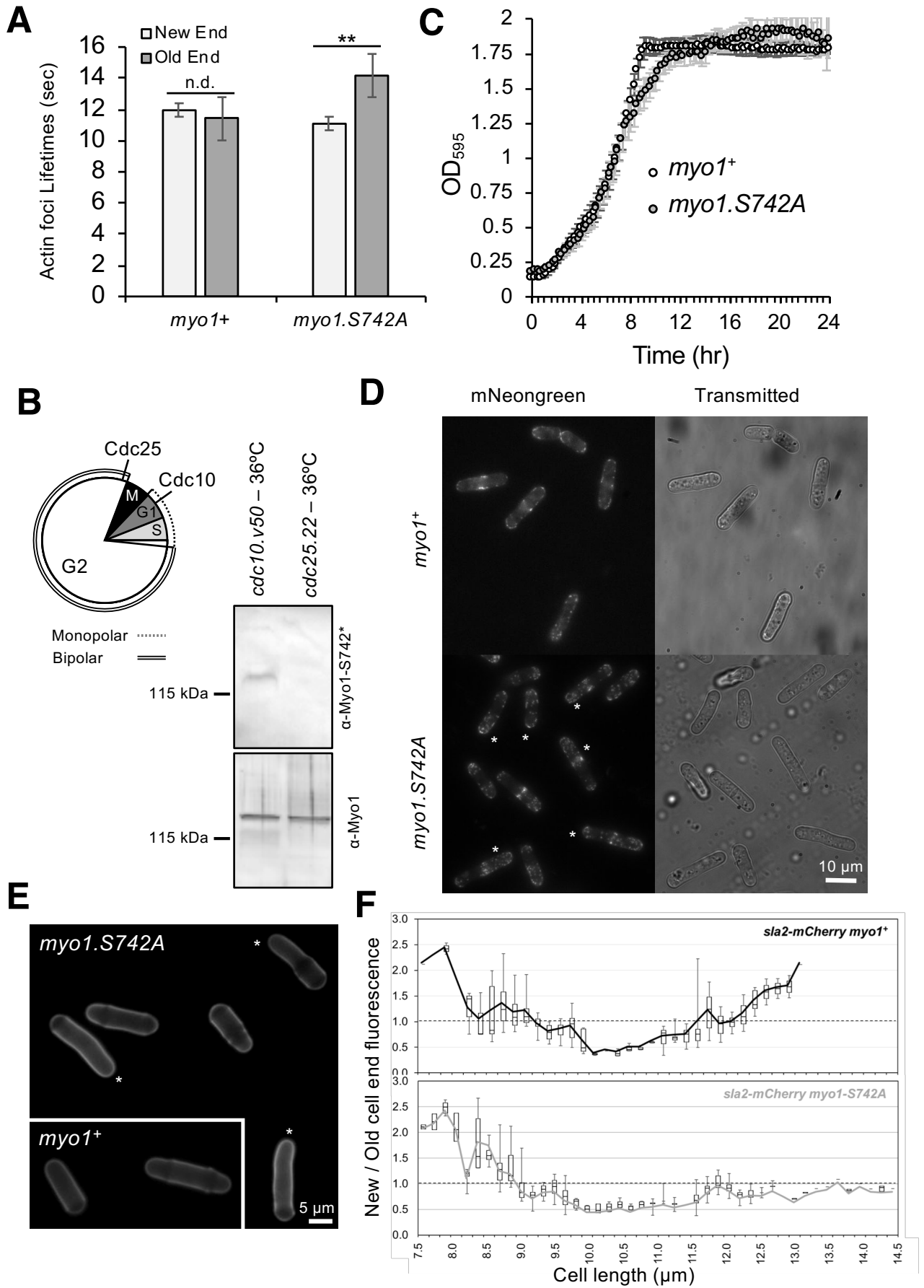


Figure 5

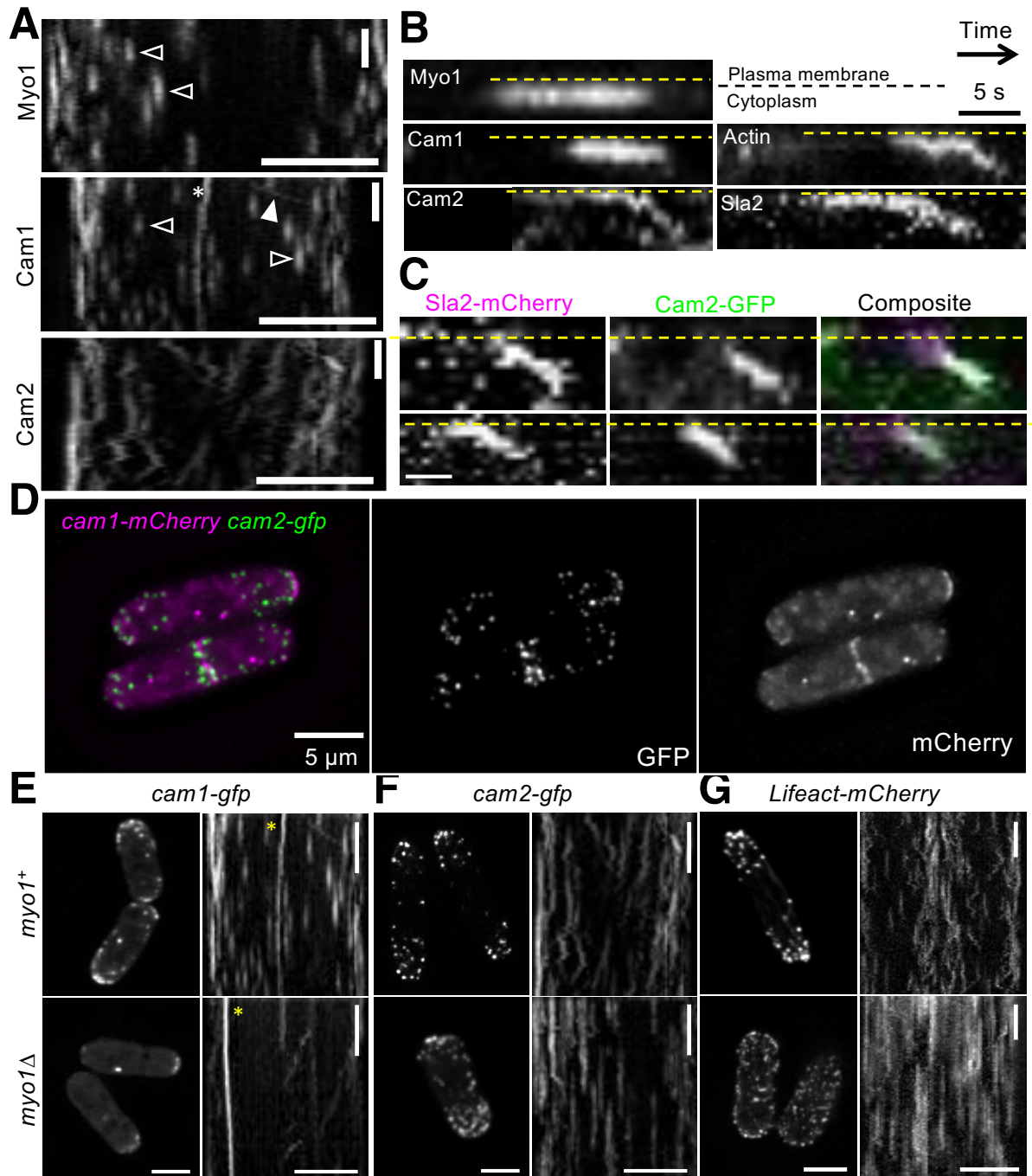


Figure 6

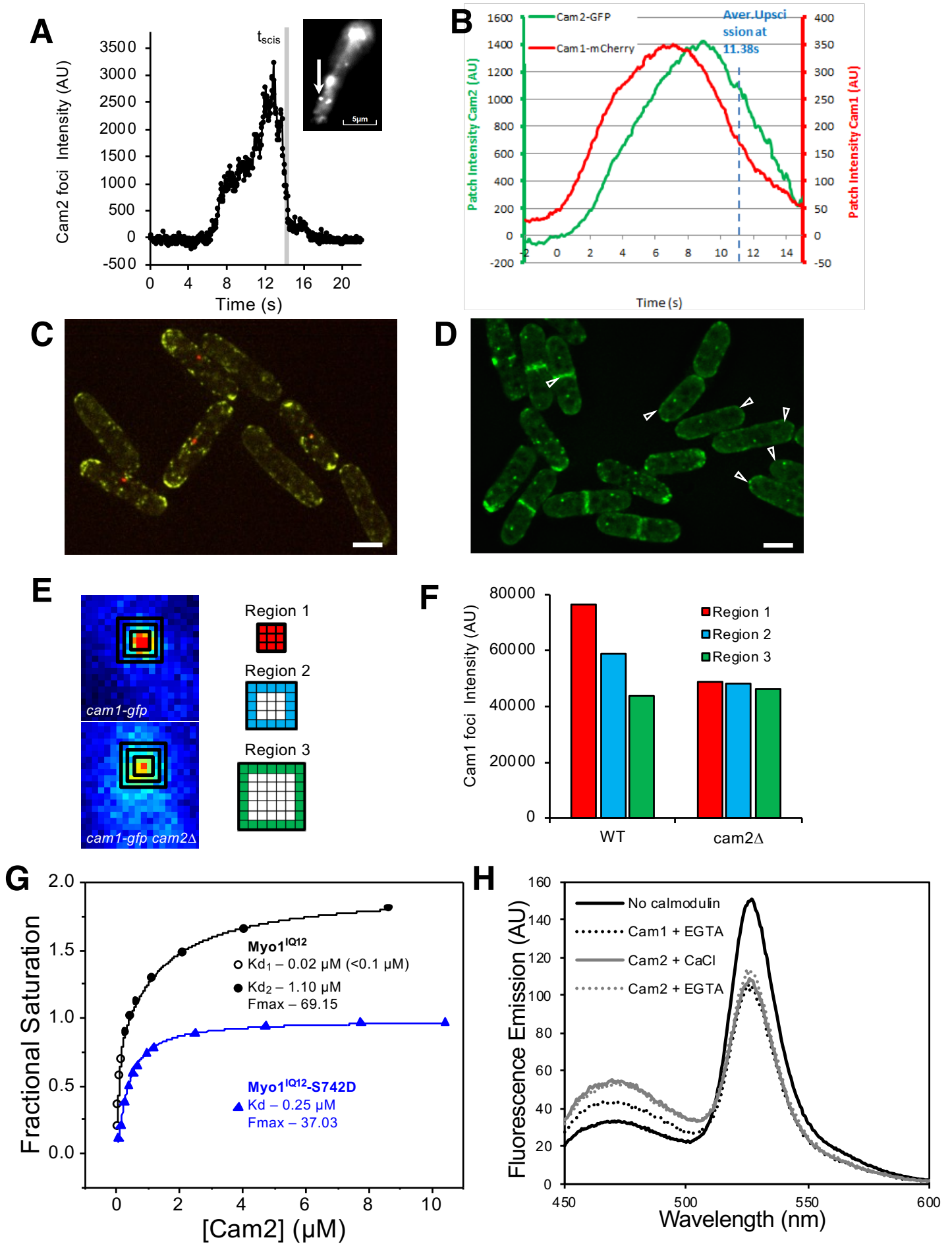


Figure 7

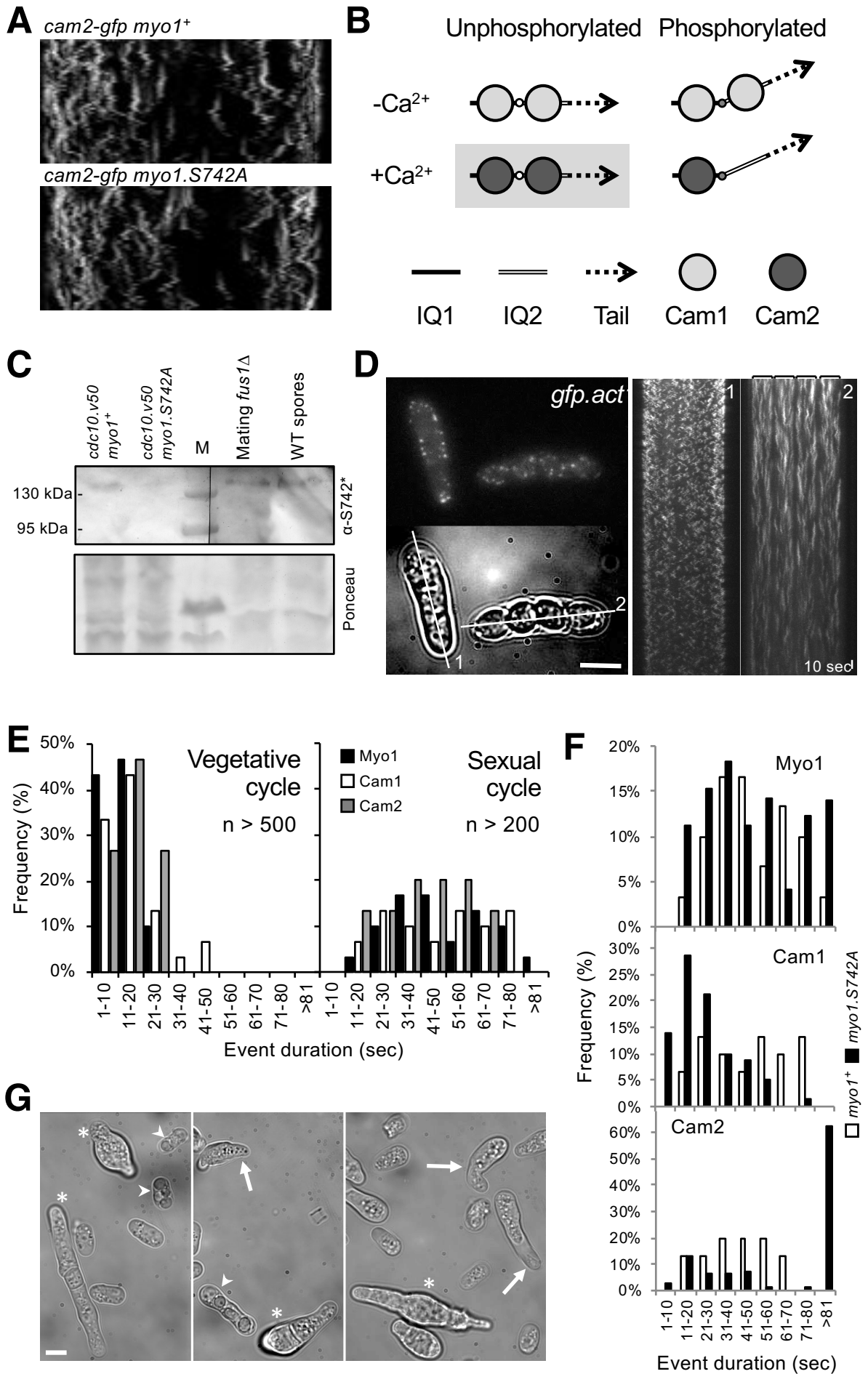
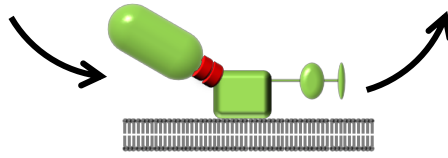
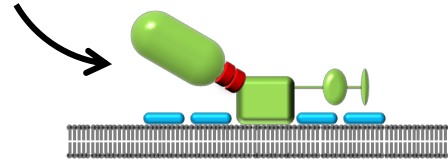


Figure 8

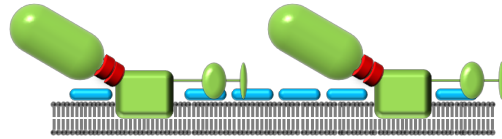
A



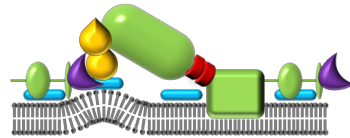
B



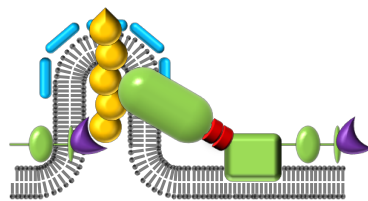
C



D



E



F

